Onset of differentiation is posttranscriptionally controlled in adult neural stem cells

Avni Baser[1], Yonglong Dang[1], Maxim Skabkin[1], Gülce S. Gülcüler Balta[1], Georgios Kalamakis[1], Susanne Kleber[1], Manuel Göpferich[1], Roman Schefzik[2], Alejandro Santos Lopez[1], Enric Llorens Bobadilla[1], Carsten Schultz[3], Bernd Fischer[2] & Ana Martin-Villalba[1]

[1] Molecular Neurobiology, German Cancer Research Center (DKFZ), Im Neuenheimer Feld 581, 69120, Heidelberg, Germany

[2] Computational Genome Biology, German Cancer Research Center (DKFZ), Im Neuenheimer Feld 580, 69120, Heidelberg, Germany

[3] Chemical Cell Biology, European Molecular Biology Laboratory (EMBL), Meyerhofstraße 1, 69117 Heidelberg, Germany

Correspondence: AMV (a.martin-villalba@dkfz-heidelberg.de)

Dedicated to the memory of Bernd Fischer

SUMMARY

The contribution of posttranscriptional regulation of gene expression to neural stem cell differentiation during tissue homeostasis remains elusive. Here we show highly dynamic changes in protein synthesis along differentiation of stem cells to neurons *in vivo*. Examination of individual transcripts using RiboTag mouse models reveals that neural stem cells efficiently translate abundant transcripts, whereas translation becomes increasingly controlled with the onset of differentiation. Stem cell generation of early neuroblasts involves translational repression of a subset of mRNAs including the stem cell-identity factors Sox2 and Pax6 as well as translation machinery components. *In silico* motif analysis identifies a pyrimidine-rich motif (PRM) in this repressed subset. A drop in mTORC1 activity at the onset of differentiation selectively blocks translation of PRM-containing transcripts. Our data uncovers how a drop in mTORC1 allows robust simultaneous posttranscriptional repression

of key stem cell identity-factors and translation-components and thereby stemness exit and migration.

To generate olfactory bulb interneurons in the adult brain, ventricle-contacting NSCs exit the dormant state to transit through a primed quiescent to an active state[1-3] and produce neurogenic progenitors (NPs). NPs differentiate into neuroblasts (NBs) that migrate along the rostral migratory stream to the olfactory bulb (OB) where they ultimately transform into new granule and periglomerular interneurons[4,5]. Maintenance of NSCs throughout the life of the animal critically depends on keeping them in a state of quiescence, which they entered during embryonic development[6,7]. This dormant state features low protein synthesis[2] that is key to maintain the pool of fully functional stem cells not only in the brain but also in the bone marrow (haematopoietic stem cells: HSCs) and hair follicles (hair follicle stem cells: HFSCs) [8-10]. With transition into the primed state, protein synthesis increases before actual division [2,8,11]. However, how protein synthesis changes along the further steps of maturation has not been studied.

Global protein synthesis is highly dynamic along stem cell differentiation to neurons

To address active protein synthesis during adult olfactory bulb neurogenesis, we FACS-isolated multiple cell populations from the ventricular-subventricular zone (SVZ) and the olfactory bulb based on their surface marker expression as previously described[2]. This strategy enables distinction between quiescent NSCs (qNSCs, GLAST$^+$PROM$^+$), active NSCs (aNSCs, GLAST$^+$PROM$^+$EGFR$^+$), neurogenic progenitors (NPs, only EGFR$^+$), early neuroblasts (ENBs, PSA-NCAM$^+$ from SVZ) and late neuroblasts (LNBs, PSA-NCAM$^+$ from OB, Fig. 1a). In addition, to overcome the challenging need of sorting neurons we isolated cells from the olfactory bulb and identified by marker expression post fixation: LNBs (DCX$^+$NeuN$^-$), early neurons (DCX$^+$NeuN$^+$) and mature neurons (DCX$^-$NeuN$^+$) (Fig. 1d). Active protein synthesis per cell was quantified by incorporation of the aa-tRNA mimic

56 homologue O-Propargyl-Puromycin (OPP) into nascent proteins[12]. We confirmed that global
57 protein synthesis is very low in qNSCs and increases dramatically in aNSCs[2] (Fig. 1b-c). In
58 addition, we identified a further increase in neurogenic progenitors and a dramatic drop in
59 ENBs back to levels found in qNSC (Fig. 1b-c). To directly assess global protein synthesis in
60 ENB that exclusively derive from NSCs we used Tlx-CreER-eYFP reporter mice. Tlx-
61 recombined population overlapped with the previously characterized GLAST+PROM+
62 population of NSC, confirming that we are looking at the same subset of cells with Tlx-
63 labeling and FACS-isolation approach (Extended data Fig. 1a,b). Reporter-positive ENBs
64 exhibited a dramatic drop in OPP incorporation as compared to NSCs, similar to the drop
65 found in FACS-isolated populations (Extended data Fig. 1c,d). Thereafter, active protein
66 synthesis increases again in LNBs, which in contrast to ENBs are postmitotic and, thus, we
67 hypothesize that this increase potentially relates to the complex process of integration into the
68 neuronal network. Altogether these data support the idea that the need to differentiate and not
69 proliferation dictates the level of protein synthesis as previously reported for HFSCs[8]. From
70 LNBs to early and mature neurons active protein synthesis gradually decreases (Fig. 1 e,f),
71 supposedly because neurons rather need local proteome changes through localized
72 translation[13]. Indeed, a recent study addressing the axonal translatome by ribotagging
73 demonstrates that a subset of mRNAs with key axon-specific functions is highly enriched in
74 axons where they are locally translated[14].
75
76 **RiboTag mouse models target distinct stages of neuronal differentiation**
77 To address how transcript-specific translation relates to transcript abundance, we developed a
78 system for parallel assessment of the transcriptome and translatome of NSCs and their
79 progeny *in situ*. We used the RiboTag mouse line that carries a hemagglutinin (HA)-tagged
80 variant of the large ribosomal subunit RPL22 (RPL22-HA)[15], one of the most stable
81 ribosomal components[16] that is localized on the exposed solvent side of 60S and is not
82 involved in either mRNA or tRNA binding or ribosomal dynamics during translation[17].

83 Ribotag mice were bred with previously established cre-inducible fluorescent reporter mouse
84 lines, allows parallel ribosomal tagging and FACS isolation of the cell population of interest.
85 We generated Tlx-CreER-Rpl22.HA-eYFP (TiCRY) and Dcx-CreER-Rpl22.HA-eYFP
86 (DiCRY) mouse lines to target NSCs and their progeny, respectively (Fig. 2a).
87 As opposed to previous studies that have used this system to study terminally differentiated
88 cells[14,15,18], targeting of cells along their maturation stages requires (i) sufficient incorporation
89 of the tagged-RPL22 in functional ribosomes and (ii) no contamination of the target-
90 maturation stage by other stages. Thus, we first confirmed that this strategy allows targeting
91 of the maturation-stage of interest by immunohistochemistry for HA, eYFP and different
92 cellular marker (Fig. 2b-d and Extended Data Fig. 2g-k). We further confirmed efficient
93 incorporation of HA-tagged RPL22 into translating ribosomes and excluded potential changes
94 in global protein synthesis levels in cultured NSCs from TiCRY mice (Extended Data Fig. 2a-
95 f). Together, this characterization shows that careful selection of the reporter mouse line,
96 timepoints and regions allows simultaneous ribosome-tagging and fluorescent-labeling of
97 four distinct cell populations *in vivo* encompassing the complete adult OB-lineage
98 progression: NSCs, ENBs, LNBs and neurons.
99
100 **RiboTag system allows parallel study of transcriptome and translatome**
101 Next, to examine the transcriptome (total RNA) and translatome (Ribosome-bound RNA) we
102 extracted the different RNA fractions from these maturation stages *in vivo*.
103 Immunoprecipitation of HA-RPL22 allowed isolation of mRNAs bound to ribosomes
104 (RIBO+). To correct for unspecific binding of mRNAs we included samples of mock
105 immunoprecipitation of SVZ or OB tissue from Cre-negative animals (RIBO-). For isolation
106 of total RNA of the same target population, we sorted eYFP^{+}-cells (RNA; Extended Data Fig.
107 3b). First we validated enrichment of the expected population-specific marker genes in the
108 RIBO+ and RNA fraction by quantitative RT-PCR (Extended Data Fig. 3a,c). Thereafter we
109 profiled the RNA from the RNA, RIBO+ and RIBO- fractions by next generation sequencing.

110 Sequencing results confirmed high enrichment for cell type specific transcripts both at the
111 level of transcriptome (RNAseq) and translatome (RIBOseq)(Fig. 3 a,b; Supplementary Table
112 1). While NSC transcripts were mostly restricted to NSCs in the SVZ, neuroblast genes were
113 already expressed at the level of NSCs (Fig. 3a). Similarly, expression of neuronal transcripts
114 started already at the immature stage of LNBs (Fig. 3b). To further investigate the
115 transcriptome and translatome, we performed differential expression analysis for stage
116 transitions solely based on RNAseq or RIBOseq data, respectively (Fig. 3c-e; Extended Data
117 Fig. 3d,e; Supplementary Tables 2, 3). Notably, the key core-regulators of neural
118 development were represented in the transcriptome and translatome throughout the transition
119 between the different differentiation stages (RNAseq and RIBOseq overlap) (Fig. 3c-e).
120 Collectively, these data demonstrate that our system can be used to obtain high purity
121 population (Extended Fig. 1c-e) and for integrated stage-specific transcriptome and
122 translatome analysis.
123
124 **Transcriptome and translatome diverge during lineage progression**
125 Intriguingly, our analysis additionally revealed the existence of subsets of genes that are
126 either less or more efficiently loaded onto ribosomes as compared to available mRNA (Fig.
127 3c-e). Besides, it showed a surprisingly low overlap between RIBO-seq and RNA-seq in the
128 transition from ENB to LNB (Fig. 3d). This is the only comparison of cells extracted from
129 two different regions, SVZ for NSC and OB for ENB, which highlighted the need of
130 normalization. Thus, in order to identify transcripts, whose binding to ribosomes is post-
131 transcriptionally controlled, we fit a linear model to explain the RIBOseq data by the RNAseq
132 data (representing default translation) and the RIBO- controls (representing background
133 binding) for each stage of interest (Fig. 4a). To identify targets with high confidence, we
134 restricted our analysis to protein coding, highly abundant transcripts (read count > 1000 in
135 RNAseq). Transcripts that were less abundant in RIBOseq compared to RNAseq (and RIBO-)
136 were entitled „repressed“, suggesting that active mechanisms prevent them from ribosome

137 association. In contrast, transcripts with higher ribosome association than expected based on
138 RNAseq data and RIBO- data were entitled „enhanced“, indicating that their ribosome
139 association is actively promoted. Our analysis revealed that abundant transcripts readily bind
140 to ribosomes in NSCs (Fig. 4b,c,f and Supplementary Table 4), indicating little post-
141 transcriptional regulation as previously reported in homeostatic HSCs[19]. Excitingly, with the
142 onset of differentiation we observed a higher divergence of transcriptome and translatome
143 (Fig. 4b,c,f, Extended Data Fig. 4a, and Supplementary Table 4). Neurons showed the highest
144 degree of uncoupling between RNAseq and RIBOseq. Notably, most analyzed genes showed
145 either repressed or enhanced translation as compared to their mRNA levels emphasizing the
146 important role of posttranscriptional regulation for neuronal differentiation and function. The
147 analysis of explained variance also confirmed that translation efficiency justifies a
148 significantly higher fraction of the RIBOseq data in neurons as compared to RNA abundance
149 (Extended Data Fig. 4b,c). We further examined the subset of transcripts sharing common
150 translational control at the different maturation stages (Fig. 4d-f). First, we observed many
151 transcripts exclusively repressed or enhanced at the ENB stage, some of which were validated
152 via western-blot (WB) and qPCR (Extended Fig. 4 d-f). Second, LNBs and neurons exhibited
153 the highest share of repressed transcripts, indicating that post-transcriptional repression of
154 translation already starts at the LNB stage and is kept in neurons. Collectively, these data
155 indicate that with differentiation to mature neurons, cells enter a mode of increasing
156 dependency on posttranscriptional control.
157
158 **Stage-specific repression of Sox2 translation**
159 We next focused on the exit of the stem-state for transitioning into migrating ENBs. This is
160 the first stage showing substantial control of ribosome binding of abundant mRNAs. Notably,
161 the subset of repressed transcripts comprised multiple ribosomal genes as well as the
162 prominent developmental transcription factors Pax6 and Sox2 (Fig. 4d). Sox2 and Pax6 have
163 a highly evolutionary conserved role in determining the stem cell identity of embryonic and

164 adult radial-glial progenitors together with Sox9[20]. In addition Sox2 is one of the factors used
165 to reprogram somatic cells into pluripotent stem cells[21]. To validate Sox2 sequencing profile
166 (Fig. 5a), we applied parallel *in situ* hybridization (ISH) for Sox2 mRNA and
167 immunohistochemistry (ICC) for Sox2 and Dcx protein in the Tlx-reporter mice. This
168 allowed simultaneous assessment of Sox2 mRNA and protein in NSCs and ENBs (Fig. 5b-d
169 and extended Fig. 5c). While both NSCs and ENBs showed substantial levels of Sox2
170 mRNA, protein expression was mostly limited to NSCs (Fig. 5c,d). Interestingly, ENBs
171 produce little Sox2 protein even when containing high levels of its mRNA. Comparison of
172 protein expression to mRNA abundance revealed a 2.8-fold reduction of Sox2 translation
173 efficiency from NSCs to ENBs. In addition, we independently confirmed that Sox2 shows
174 highest translation efficiency in NSCs as compared to NPs and ENBs in freshly sorted SVZ
175 cells via ISH and ICC but also via WB and qRT-PCR (Fig. 5e and Extended Data Fig. 5a-d).
176 Interestingly, NPs, whose maturation state lies between NSCs and ENBs, show an
177 intermediate efficiency for Sox2 translation (see regression lines), even if they displayed the
178 highest absolute levels of Sox2 mRNA and protein. These data demonstrate a gradual
179 repression of Sox2 translation in the transition from NSCs through NPs to ENBs.
180 Interestingly, Sox2-mRNA regains binding to ribosomes later in LNBs and neurons (Fig. 5a).
181 Thus, we further validated Sox2 translation in newborn neurons using DiCRY mice. While,
182 adult born neurons in the granular cell layer did not show any Sox2 protein expression,
183 periglomerular neurons exhibited high levels of Sox2 protein (Fig. 5f,g). Indeed, we identified
184 Calretinin-positive newborn periglomerular neurons as the only neurons in the olfactory bulb
185 expressing Sox2 protein (Fig. 5f,g). Thus, translation of Sox2 transcripts is transiently
186 repressed in ENBs and becomes re-expressed in a subset of newborn olfactory bulb neurons.
187 We next asked whether the set of 282 translationally repressed transcripts in ENBs would
188 share distinct features as compared to non-repressed transcripts. *De novo* motif analysis on
189 both untranslated regions (UTRs) as well as coding region of repressed transcripts discovered
190 enriched motifs in the 5' UTR including a stretch of pyrimidines (TCTTTC/CTCTTT,

191 Supplementary Table 5) that we coined pyrimidine rich motifs (PRMs). A stretch of
192 pyrimidines is also found in 5' terminal oligopyrimidine (TOP) motifs, which are particularly
193 sensitive to translation-mediated by mTORC1 activity[22]. Unlike the classical TOP motifs, this
194 PRM is not always located at the terminal end of 5'UTR. Similarly to TOP-containing
195 transcripts, PRM was found in transcripts encoding components of the translation machinery,
196 such as ribosomal proteins (Fig. 6a, Extended Data Fig. 6a). Interestingly, PRM-containing
197 transcripts were not repressed at the LNB stage despite the higher number of translationally
198 repressed transcripts at this stage (Fig. 6b). Thus, we hypothesized that mTORC1 activity
199 might be low in ENBs and high in NSCs and LNBs. This assumption is in conflict with the
200 reported phosphorylation of 40S ribosomal protein S6 (rpS6), used as readout of mTORC1
201 activity, in proliferating neuroblast, but not in SVZ-neural stem cells[23]. In order to visualize
202 phosphorylation of rpS6 specifically in NSCs and ENBs *in situ*, we used the Tlx-CreER^{T2}-
203 eYFP reporter mouse in combination with immunofluorescence staining for Dcx. Notably,
204 phosphorylation of rpS6 (pS6) was low in all ENBs while NSCs showed heterogeneous levels
205 of pS6, probably reflecting their different activation status (Fig. 6c). We further assessed
206 expression of mTOR-related factors in freshly isolated ENBs and NSCs via WB. As predicted
207 from the Ribo-seq analysis (see supplemental material), ENBs exhibited a downregulation of
208 pS6 and phosphorylated-p70-S6K, and of total TSC2 and Rheb as compared to NSCs (Fig.
209 6d). In contrast, LNBs in the olfactory bulb showed significantly higher levels of pS6 than
210 neigbouring neurons (Extended Data Fig. 6f). Interestingly, neurons of the mitral cell layer in
211 the olfactory bulb showed high pS6 levels (data not shown), suggesting variability between
212 different neuronal subtypes regarding mTOR activity, which might translate into protein
213 synthesis rates. Thus, the drop of mTORC1 in ENBs but not LNBs could be the reason for the
214 specific repression of PRM-transcripts in ENBs. To experimentally validate the role of
215 mTORC1 in translation of the PRM-transcript Sox2 *in vivo*, freshly isolated ENBs were
216 acutely treated with membrane permeant phosphatidylinositol 3,4,5-trisphosphate
217 [PI(3,4,5)P3]. This lipid is produced upon nutrients and growth factor activation of PI3K and

218 mediates AKT activation of mTORC1[24]. ENBs were either treated with PI(3,4,5)P3 alone or
219 together with the mTOR inhibitor Torin1, which unlike rapamycin fully inhibits
220 mTORC1[22,25]. Thereafter, levels of pS6 and Sox2 proteins were assesed by ICC in single
221 cells. First, this assay confirmed that NSCs exhibit higher levels of pS6 and Sox2 than ENBs
222 (Fig. 6e). Second, exposure of ENBs to PI(3,4,5)P3 highly increased pS6 levels in ENBs to
223 levels comparable to NSCs (Fig. 6e). PI(3,4,5)P3-mediated pS6 increased could be inhibited
224 by Torin. Most importantly, PI(3,4,5)P3 also increased Sox2-protein levels in a mTORC1-
225 dependent manner, as Sox2 protein expression could be repressed by Torin (Fig. 6e). Next,
226 we wanted to examine the mTORC1-dependent rate of ribosomal load of PRM+ and PRM-
227 transcripts. To this end we turned to NSCs cultures to increase the input material and be able
228 to gain cell-fractions with distinct ribosome content via sucrose gradient fractionation of
229 Torin1- or vehicle-treated NSCs. Most PRM+ transcripts but not PRM- ones, shifted to the
230 lighter fractions upon Torin1-treatment, indicating that their translation depends on mTORC1
231 activity (Extended Data Fig. 6d). Surprisingly, this shift could not be detected for Sox2-
232 transcripts (Extended Data Fig. 6d,e). Therefore we compared the expression of mTORC-
233 related factors in cultured NSCs to expression in freshly isolated NSCs and ENBs. In cultured
234 NSCs were left untreated or treated with Torin or the EGFR inhibitor, erlotinib. The latter
235 was used to mimick the loss of EGFR occurring in NSCs transitioning to ENBs. Both Torin
236 and Erlotinib treatment of NSCs *in vitro* led to a transient reduction in pS6 and
237 phosphorylated-p70S6K, but not to lowering expression of the mTORC1-activator Rheb as
238 found between freshly isolated ENBs and NSCs (Fig. 6d and Extended Fig. 6 b,c). These
239 findings suggest that lineage transitions induced stoichiometric changes that cannot be
240 achieved by an acute inhibition of mTORC1. Surprisingly, Torin-treated cultured NSCs
241 exhibited a slight upregulation of protein expression of genes exhibiting enhanced translation
242 efficiency in the transition from NSCs to ENBs *in vivo* (Extended Fig. 6 e). These genes are
243 overrepresented in the neuron-differentiation- related gene ontology categories (Extended Fig.
244 6a). Thus, these data suggest that a drop of mTORC1 orchestrates posttranscriptional

245 repression of stemness and enhancement of neuronal differentiation processes. Along this
246 line, long-term activation of mTORC1 via deletion of TSC2 in human embryonic stem cells
247 generated neurons with increased expression of neural stem cell and proliferation markers
248 including SOX2, Nestin and PDNA and decreased expression of neuronal markers[26].
249 Altogether these data underline the importance of studying the molecular underpinnings of
250 lineage transitions *in vivo* and unveils a yet unrecognized differential sensitivity of targets to
251 long-term and short-term mTORC1 inhibition that needs to be addressed in future studies.
252 Thus, our data uncovers a way of regulation of components of the translation machinery and
253 neurogenic transcription factors via modulation of mTORC1-activity in the natural
254 environment of the brain. An activation of mTORC1-activity is found in injured muscle stem
255 cells, which transit from a quiescent (G0) to a quiescent primed state to finally enter cell cycle
256 (G alert)[11]. Yet the specific transcripts underlying mTORC1-control of G alert in muscle cells
257 remain unknown. Most importantly, this might represent a more general mechanism by which
258 mTOR controls stemness.
259
260 DISCUSSION
261 Altogether, this study demonstrates that the rate of active protein synthesis is tightly
262 controlled during stem cell differentiation into neurons. This general activation of protein
263 synthesis is required to exit the dormant state in NSCs[2] and muscle stem cells[11] and to activate
264 differentiation in skin stem cells[8] and drosophila germline stem cells[27]. Notably, impaired
265 drop of mTORC1 by deletion of TSC1 in single SVZ-NSC in the rodent brain, led to
266 generation of Dcx-negative cells with immature radial-like morphology that were unable to
267 migrate out of the SVZ[28]. Our data indicates that the observed impaired neurogenesis is due to
268 loss of translation arrest in ENBs needed to repress stem cell identity prior to a re-
269 establishment of protein synthesis in LNBs to allow neuronal maturation. There has been
270 long-standing discussions about the overall correlation of transcript- and protein abundance
271 with contradicting conclusions from identical datasets[29,30]. However, with the forthcoming of

272 refined mathematical models and latest technologies for quantification, it is believed that
273 mRNA levels largely explain protein abundance during steady state[31]. Notably, the study of
274 developmental lineage transitions *in vivo*, has allowed us to uncover a highly dynamic and
275 stage-specific regulation of translation efficiency. Whereas the transcriptome and translatome
276 highly correlate in stem cells during homeostasis, they become increasingly divergent with
277 the exit of the stemness state. The relatively large number of repressed mRNAs in our system
278 is not surprising if we remember that stem cells partially recapitulate some features of germ
279 cells, and the latter rely considerably on translational regulation instead of transcriptional
280 during most of their lifespan. Furthermore, recent data revealed embryonic origin of adult
281 NSCs[6,7]. The stock of mRNAs in the cytoplasm, stable but not translated, allows the cell to
282 respond quickly to stimuli. NSCs rearrange their morphology, contacts with the niche and
283 migrate to a new niche upon their differentiation. Thus, for such cells relying on post-
284 translational regulation might be crucial to be able to quickly adapt to fast-changing
285 environment conditions. Importantly, selective changes in translation efficiency have been
286 reported in oncogenic NSC in a spontaneous brain tumor model[32].
287 In early neuroblasts, a drop in mTORC1 activity programs a transient arrest in translation of
288 PRM+ transcripts, which include ribosomal genes and key evolutionary conserved
289 determinants of stem cell identity. Exit of stemness requires tight regulation to ensure
290 continuos production of differentiated progeny while maintaining the pool of stem cells.
291 Dysregulation of this transition is found in aging and cancer[33]. mTOR is hyperactivated in
292 90% of glioblastomas[34]. Notably, mTOR inhibition by rapamycin in glioblastoma abrogated
293 expression of Sox2 protein thereby reversing their chemoresistance to temozolomide[35]. Thus,
294 this study uncovers an unrecognized role of mTOR in stem cells that together with activation
295 of a G-alert state and proliferation contributes to explain the dependency of cancer stem cells
296 on mTOR activity. Besides, we identify a biological process in the adult brain *in vivo* that
297 critically depends on the selective sensitivity of PRM+ transcripts to mTOR-mediated
298 translation. Likewise, despite loss of mTORC activity, a subset of mRNAs increased their

translation efficiency. The main effect of mTOR on translation is the phosphorylation and inactivation of 4EBP proteins, which associate and inactivate a cap-binding initiation factor eIF4E responsible for 40S subunit recruitment to mRNAs. Those mRNAs, showing high dependence on the cap structure and eIF4E, are among the most sensitive to mTOR activity. Many such mTOR-sensitive mRNAs encode the most abundant proteins in cells, including ribosomal proteins. These mRNAs are very efficient in translation and form a class of so-called "strong" mRNAs[36]. However, the advent of the next-generation sequencing technology revealed a considerable number of mRNAs, which show resistance to mTOR repression and even get stimulated[22,37]. Additional studies found out that many such mRNAs are less dependent on eIF4E and can apply other mechanisms of 40S recruitment independent on the eIF4E-cap interaction[38]. These mRNAs could use isoforms of initiation factors eIF4E and eIF4G, which do not bind 4EBP repressors and could confer less dependence on mTOR to the corresponding mRNAs. Furthermore, these mRNAs being less competitive upon optimal conditions get considerable advantages upon the repression of "strong" mRNAs, relishing uncompetitive availability of ribosomes, tRNAs, and translation factors. Although, the specific elements of such mRNAs providing mTOR independence are not yet well described, recently discovered capability of N6-methylated adenines localized in the 5'-UTRs to directly attach 40S in an eIF4E-independent manner might be one of those[39].Our motif analysis solely revealed enrichment in the coding region of a consensus motif for m6A "CGCAAC" (as shown in table S5), though this is not sufficient to explain escape from mTORC1 inhibition. Future studies of N-6-methylated adenines should further our understanding of increased translation efficiency in the frame of low mTORC1 activity for this set of transcripts.

In summary, our data offers a comprehensive genomic view on translational control during neuron generation in the adult brain, adding a novel layer to our knowledge of the molecular mechanisms controlling stem cell differentiation.

326
327
328
329
330
331
332
333
334
335
336
337
338
339
340
341
342
343
344 REFERENCES

345 1 Codega, P. *et al.* Prospective Identification and Purification of Quiescent
346 Adult Neural Stem Cells from Their In Vivo Niche. *Neuron* **82**, 545-559,
347 doi:10.1016/j.neuron.2014.02.039 (2014).
348 2 Llorens-Bobadilla, E. *et al.* Single-Cell Transcriptomics Reveals a
349 Population of Dormant Neural Stem Cells that Become Activated upon
350 Brain Injury. *Cell Stem Cell* **17**, 329-340 (2015).
351 3 Mich, J. K. *et al.* Prospective identification of functionally distinct stem
352 cells and neurosphere-initiating cells in adult mouse forebrain. *eLife* **3**,
353 894, doi:10.7554/eLife.02669 (2014).
354 4 Bayraktar, O. A., Fuentealba, L. C., Alvarez-Buylla, A. & Rowitch, D. H.
355 Astrocyte development and heterogeneity. *Cold Spring Harb Perspect Biol*
356 **7**, a020362, doi:10.1101/cshperspect.a020362 (2015).
357 5 Ming, G. L. & Song, H. Adult neurogenesis in the mammalian brain:
358 significant answers and significant questions. *Neuron* **70**, 687-702 (2011).

6 Fuentealba, L. C. *et al.* Embryonic Origin of Postnatal Neural Stem Cells. *Cell* **161**, 1644-1655, doi:10.1016/j.cell.2015.05.041 (2015).
7 Furutachi, S. *et al.* Slowly dividing neural progenitors are an embryonic origin of adult neural stem cells. *Nat Neurosci* **18**, 657-665, doi:10.1038/nn.3989 (2015).
8 Blanco, S. *et al.* Stem cell function and stress response are controlled by protein synthesis. *Nature* **534**, 335-340, doi:10.1038/nature18282 (2016).
9 Signer, R. A. J., Magee, J. A., Salic, A. & Morrison, S. J. in *Nature* Vol. 509 49-54 (2014).
10 Bonaguidi, M. A. *et al.* In vivo clonal analysis reveals self-renewing and multipotent adult neural stem cell characteristics. *Cell* **145**, 1142-1155 (2011).
11 Rodgers, J. T. *et al.* mTORC1 controls the adaptive transition of quiescent stem cells from G0 to G(Alert). *Nature* **510**, 393-396 (2014).
12 Liu, J., Xu, Y., Stoleru, D. & Salic, A. in *Proc. Natl. Acad. Sci. U.S.A.* Vol. 109 413-418 (2012).
13 Jung, H., Yoon, B. C. & Holt, C. E. Axonal mRNA localization and local protein synthesis in nervous system assembly, maintenance and repair. *Nature Reviews Neuroscience* (2012).
14 Shigeoka, T. *et al.* in *Cell* Vol. 166 181-192 (2016).
15 Sanz, E. *et al.* in *Proc. Natl. Acad. Sci. U.S.A.* Vol. 106 13939-13944 (2009).
16 Shi, Z. *et al.* Heterogeneous Ribosomes Preferentially Translate Distinct Subpools of mRNAs Genome-wide. *Mol Cell* **67**, 71-83 e77, doi:10.1016/j.molcel.2017.05.021 (2017).
17 Anger, A. M. *et al.* Structures of the human and Drosophila 80S ribosome. *Nature* **497**, 80-85, doi:10.1038/nature12104 (2013).
18 Sanz, E. *et al.* RiboTag analysis of actively translated mRNAs in Sertoli and Leydig cells in vivo. *PLoS One* **8**, e66179, doi:10.1371/journal.pone.0066179 (2013).
19 Cabezas-Wallscheid, N. *et al.* in *Stem Cell* 1-16 (Elsevier Inc., 2014).
20 Camp, J. G. *et al.* Human cerebral organoids recapitulate gene expression programs of fetal neocortex development. *Proc Natl Acad Sci U S A* **112**, 15672-15677, doi:10.1073/pnas.1520760112 (2015).
21 Yamanaka, S. Pluripotency and nuclear reprogramming. *Philos.Trans.R.Soc.Lond B Biol.Sci.* **363**, 2079-2087 (2008).
22 Thoreen, C. C. *et al.* in *Nature* Vol. 485 109-113 (2012).
23 Paliouras, G. N. *et al.* Mammalian Target of Rapamycin Signaling Is a Key Regulator of the Transit-Amplifying Progenitor Pool in the Adult and Aging Forebrain. *The Journal of neuroscience : the official journal of the Society for Neuroscience* **32**, 15012-15026 (2012).
24 Demetriades, C., Doumpas, N. & Teleman, A. A. Regulation of TORC1 in response to amino acid starvation via lysosomal recruitment of TSC2. *Cell* **156**, 786-799, doi:10.1016/j.cell.2014.01.024 (2014).
25 Thoreen, C. C. *et al.* in *J. Biol. Chem.* Vol. 284 8023-8032 (2009).
26 Costa, V. *et al.* mTORC1 Inhibition Corrects Neurodevelopmental and Synaptic Alterations in a Human Stem Cell Model of Tuberous Sclerosis. *Cell Rep* **15**, 86-95, doi:10.1016/j.celrep.2016.02.090 (2016).

407 27 Sanchez, C. G. *et al.* Regulation of Ribosome Biogenesis and Protein
408 Synthesis Controls Germline Stem Cell Differentiation. *Cell Stem Cell* **18**,
409 276-290, doi:10.1016/j.stem.2015.11.004 (2015).
410 28 Feliciano, D. M., Quon, J. L., Su, T., Taylor, M. M. & Bordey, A. Postnatal
411 neurogenesis generates heterotopias, olfactory micronodules and cortical
412 infiltration following single-cell Tsc1 deletion. *Hum Mol Genet* **21**, 799-
413 810, doi:10.1093/hmg/ddr511 (2012).
414 29 Li, J. J., Bickel, P. J. & Biggin, M. D. System wide analyses have
415 underestimated protein abundances and the importance of transcription
416 in mammals. *PeerJ* **2**, e270, doi:10.7717/peerj.270 (2014).
417 30 Schwanhausser, B. *et al.* Global quantification of mammalian gene
418 expression control. *Nature* **473**, 337-342 (2011).
419 31 Li, J. J. & Biggin, M. D. in *Science* Vol. 347 1066-1067 (2015).
420 32 Gonzalez, C. *et al.* Ribosome Profiling Reveals a Cell-Type-Specific
421 Translational Landscape in Brain Tumors. *The Journal of neuroscience :*
422 *the official journal of the Society for Neuroscience* **34**, 10924-10936
423 (2014).
424 33 Sahin, E. & DePinho, R. A. Axis of ageing: telomeres, p53 and
425 mitochondria. *Nat Rev Mol Cell Biol* **13**, 397-404, doi:10.1038/nrm3352
426 (2012).
427 34 Wei, W. *et al.* in *Cancer Cell* Vol. 29 563-573 (2016).
428 35 Garros-Regulez, L. *et al.* mTOR inhibition decreases SOX2-SOX9 mediated
429 glioma stem cell activity and temozolomide resistance. *Expert Opin Ther*
430 *Targets* **20**, 393-405, doi:10.1517/14728222.2016.1151002 (2016).
431 36 Pelletier, J., Graff, J., Ruggero, D. & Sonenberg, N. Targeting the eIF4F
432 translation initiation complex: a critical nexus for cancer development.
433 *Cancer Res* **75**, 250-263, doi:10.1158/0008-5472.CAN-14-2789 (2015).
434 37 Hsieh, A. C. *et al.* The translational landscape of mTOR signalling steers
435 cancer initiation and metastasis. *Nature* **485**, 55-61,
436 doi:10.1038/nature10912 (2012).
437 38 Shatsky, I. N., Dmitriev, S. E., Andreev, D. E. & Terenin, I. M.
438 Transcriptome-wide studies uncover the diversity of modes of mRNA
439 recruitment to eukaryotic ribosomes. *Crit Rev Biochem Mol Biol* **49**, 164-
440 177, doi:10.3109/10409238.2014.887051 (2014).
441 39 Meyer, K. D. & Jaffrey, S. R. Rethinking m6A Readers, Writers, and Erasers.
442 *Annu Rev Cell Dev Biol*, doi:10.1146/annurev-cellbio-100616-060758
443 (2017).
444 40 Liu, H. K. *et al.* The nuclear receptor tailless is required for neurogenesis
445 in the adult subventricular zone. *Genes Dev.* **22**, 2473-2478 (2008).
446 41 Werner, L. *et al.* Involvement of doublecortin-expressing cells in the
447 arcuate nucleus in body weight regulation. *Endocrinology* **153**, 2655-2664
448 (2012).
449 42 Retz, K. C. & Steele, W. J. in *Life Sci.* Vol. 27 2601-2604 (1980).
450 43 Mirzadeh, Z., Doetsch, F., Sawamoto, K., Wichterle, H. & Alvarez-Buylla, A.
451 in *JoVE* (2010).
452 44 Picelli, S. *et al.* in *Nat Protoc* Vol. 9 171-181 (2014).
453 45 Dinkel, C., Moody, M., Traynor-Kaplan, A. & Schultz, C. Membrane-
454 Permeant 3-OH-Phosphorylated Phosphoinositide Derivatives. *Angew*

Chem Int Ed Engl **40**, 3004-3008, doi:10.1002/1521-3773(20010817)40:16<3004::AID-ANIE3004>3.0.CO;2-O (2001).
46 Lou, W. P., Baser, A., Klussmann, S. & Martin-Villalba, A. In vivo interrogation of central nervous system translatome by polyribosome fractionation. *J.Vis.Exp.* (2014).
47 Dobin, A. *et al.* in *Bioinformatics* Vol. 29 15-21 (2013).
48 Li, B. & Dewey, C. N. in *BMC Bioinformatics* Vol. 12 323 (2011).
49 Love, M. I., Huber, W. & Anders, S. in *Genome Biol.* Vol. 15 550 (2014).
50 Ritchie, M. E. *et al.* in *Nucleic Acids Research* Vol. 43 e47 (2015).

Acknowledgements

We thank S. Wolf from the DKFZ Genomics and Proteomics Core Facility; V. Eckstein from the Heidelberg University Hospital FACS Core Facility; Monika Langlotz from the ZMBH FACS Core Facility, Hai-Kun Liu for Tlx-CreER and tdTomato-flox mice; Markus Schwaninger for Dcx-CreER^{T2} mice; David Wiest for the Rpl22 antibody; Klara Zwadlo, Stefanie Limpert and Katrin Volk for technical assistance; Damir Krunic and the Light Microscopy Core Facility for support with image analysis; Bernd Bukau and Günther Kramer for advice during the early stage of the project, the TAC members Aurelio Teleman, Georg Stöcklin and Matthias Hentze and the members of the Martin-Villalba laboratory for critical comments. We specially thank Aurelio Teleman for critical reading of the manuscript. This work was supported by the University of Heidelberg and DKFZ (bridge-project ZMBH-DKFZ alliance), the DFG (SFB873), the BMBF and the DKFZ.

Author contributions

Project concept, A.M.-V, A.B.; Investigation, AB, Y.D., M.S., G.S.G.B., G.K., S.K., M.G., A.S.L., E. LL.B., R.S., B.F.; Writing-Review & Editing, A.M.V., B.F., A.B.; Supervision, A.M.-V., and B.F.; Project Oversight, A.M.V., B.F.

Author information

RNAseq, RIBOseq and RIBO- raw sequence data is available from GEO (Accession number: GSE94991). Complete documented software is available as supplementary file. The complete

487 R/Bioconductor software package will be made available upon acceptance on the authors'
488 webpage (https://martin-villalba-lab.github.io/). The authors declare no competing financial
489 interests. Correspondence and requests for materials should be addressed to AMV (a.martin-
490 villalba@dkfz-heidelberg.de).
491
492 METHODS
493 **Mice**
494 Male transgenic mice of DiCRY (Dcx-CreER-Rpl22.HA-eYFP) and TiCRY (Tlx-CreER-
495 Rpl22.HA-eYFP) lines were used between 8 and 12 weeks of age for all sequencing
496 experiments. These mice were generated by mating of RiboTag mice (B6N.129-
497 Rpl22tm1.1Psam/J, purchased from The Jackson Laboratory) with Tlx-CreER-eYFP mice[40]
498 or Dcx- CreER-eYFP mice[41]. Additionally, TiCROMATO mice (Tlx-CreER-Rpl22.HA-
499 Tomato) were used whenever eYFP expression was considered to be too weak. All mice were
500 backcrossed to a C57BL/6 background.
501 All further experiments using transgenics were conducted using both male and female mice
502 up to 16 weeks of age. Recombination was induced by oral gavage of tamoxifen (TAM,
503 Sigma-Aldrich) at a concentration of 200mg/kg body weight (volume ~100µL; solved in 90%
504 sunflower oil/10% EtOH). TAM was administered twice per day for a total of 2-3 injections
505 and the experiments were conducted 3-4 days after recombination, since ribosome turnover in
506 the brain takes several days[42]. The conditions varied slightly between mouse lines due to
507 recombination efficiencies and total number of cells.
508 C57BL/6 male mice between 8 and 12 weeks of age were used for all other experiments. All
509 mice were bred inhouse at the DKFZ Center for Preclinical Research. Animals were housed
510 under standard conditions and fed ad libitum. All procedures were in accordance with the
511 DKFZ guidelines and approved by the Regierungspräsidium Karlsruhe.
512
513 **Cell sorting**

514 Animals were sacrificed by cervical dislocation and brains were immediately placed on ice.
515 The lateral SVZ was microdissected as a wholemount as previously described[43], further the
516 olfactory bulb were dissected. Tissue of 1-2 mice was used per replicate (SVZ or OB) for
517 sequencing experiments. Tissue of up to five mice was pooled per sample for OPP
518 experiments. Tissue was digested with trypsin and DNase according to the Neural Tissue
519 Dissociation kit in a Gentle MACS Dissociator (Miltenyi). For sequencing experiments
520 endogenous eYFP fluorescence was used to identify cells of interest. For OPP experiments
521 cells were sorted as previously described[2] using following antibodies: GLAST (ACSA-1)-PE
522 (Miltenyi, 1:20), APC-Cy™ 7 CD45 (BD, 1:200), O4-APC (Miltenyi, 1:50), Prominin
523 PerCP-eFluor710 (eBioscience, 1:75), PSA-NCAM-PE-Vio770 (Miltenyi, 1:50), conjugated
524 EGF-Alexa488 (Life Technologies, 1:100). During cell sorting, Sytox blue (Thermo Fisher
525 Scientific, 1:1000) was used to exclude dead cells. For transcriptome analysis, 200-500 cells
526 were sorted directly into Picopure lysis buffer (Thermo Fisher Scientific). Sequencing
527 libraries were prepared as described in the following section for immunoprecipitation
528 samples.
529
530 **RiboTag immunoprecipitation and sequencing**
531 RiboTag immunoprecipitation was conducted essentially following the original protocol[15]
532 with minor modifications. Animals were perfused with Hank's Balanced Salt Solution
533 (HBSS) supplemented with the translation inhibitor cycloheximide (CHX, 200 µg/ml) for
534 stabilization of RNA-ribosome complexes. Tissue of interest was dissected and placed in
535 tubes containing 1.4mm ceramic beads (PEQLAB). Homogenization buffer (50mM Tris HCl,
536 100mM KCl, 12mM Mg_2Cl, 1% NP-40, 1mM DTT, 1x Roche complete protease inhibitor,
537 200U/mL RNAsin from Promega, 100µg/mL CHX, 1mg/mL Heparin) was added to a weight
538 per volume ratio of 3% (e.g. 0.015g in 500µL) and tissue was homogenized using Minilys
539 Personal Homogenizer (Bertin Instruments). Samples were centrifuged and supernatant was
540 used for immunoprecipitation. Anti-HA antibody (Covance, 1:100) was added for four hours
541 (indirect conjugation) following addition of Protein G magnetic beads (100µL, prewashed

542 with homogenization buffer, Thermo Fisher Scientific) and overnight incubation (all steps at
543 4°C). Supernatant was discarded and beads were washed three times for ten minutes in high
544 salt buffer (50mM Tris HCl, 300mM KCl, 12mM Mg_2Cl, 1% NP-40, 1mM DTT, 100µg/mL
545 CHX). Finally, beads were resuspended in Picopure lysis buffer (supplemented with β-
546 mercaptoethanol, 10µL/1mL, Sigma) and RNA was isolated by Picopure RNA isolation kit
547 (Thermo Fisher Scientific) following the manufacturer's protocol. For enrichment analysis,
548 fraction of the RNA was converted to cDNA using the SuperScript VILO kit (Thermo Fisher
549 Scientific). Sequencing libraries were prepared using Smart-seq2 technology as previously
550 described[44]. Reverse transcription was performed using an oligo (dT) primer and a locked
551 nucleic acid (LNA)-containing template-switching oligonucleotide (Exiqon). Full-length
552 cDNAs were amplified by 15-18 cycles of PCR using KAPA HiFi DNA polymerase (KAPA
553 biosystems). cDNAs were then converted into libraries for Illumina sequencing according to
554 the Nextera XT Sample Preparation (Illumina) protocol. Samples were sequenced in an
555 Illumina HiSeq 2000.
556
557 **Cell culture**
558 For NSC isolation, 8-12 week old wild type C57BL/6 or TiCRY mice (one week post
559 induction) were sacrificed by cervical dislocation. A wholemount of the SVZ was
560 microdissected[43] and cells were isolated using trypsin (or papain) and DNAse according to the
561 Neural Tissue Dissociation kit in a Gentle MACS Dissociator (Miltenyi). NSCs were cultured
562 in Neurobasal medium (Thermo Fisher Scientific) supplemented with 20 ng/ml of basic
563 fibroblast growth factor bFGF and epidermal growth factor EGF.
564 Freshly sorted cells for OPP administration (translation analysis) or RNA *in situ* hybridization
565 were plated in Poly-D-lysine- and laminin-coated Lab-Tek chambers (Thermo) in Neurobasal
566 medium lacking growth factors. OPP was added to the culture (50µM) two hours after plating
567 and one hour after incubation cells were fixed for 20min using 2% paraformaldehyde (PFA)
568 in the medium. For RNA *in situ* hybridization cells were fixed for 20min using 2% PFA in the
569 medium two hours after plating.

570

571 **Erlotinib, Torin1 and** PI(3,4,5)P3 **treatment**

572 Primary NSCs were exposed to erlotinib (5 µM, stock in DMSO; SIGMA-Aldrich) or Torin1
573 (250 nM, stock in DMSO) for the indicated time periods. The solvent DMSO was used as a
574 vehicle control. Thereafter cells were collected in lysis buffer and analyzed by western blot.
575 For the PI(3,4,5)P3 (PIP3) treatment, NSCs and ENBs were sorted from SVZ and either
576 resuspended in Neurobasal media with the growth factors or fixed with 2% PFA. Thereafter,
577 ENBs were either treated with PIP3 or PIP3/Torin1. Torin1 (250nM) treatment was done for
578 5 min prior to PIP3 stimulation. PIP3/AM(DOG) synthesized as previously described[45], was
579 prepared as a stock solution of 50mM in DMSO and stored at −80°C. Just before used PIP3
580 was mixed with 20% pluronic F-127/DMSO solution (Invitrogen) in a 1:0.5 ratio to facilitate
581 cell entry. The PIP3/AM/pluronic/DMSO mixture was resuspended in 50µl ENB-medium to
582 a final concentration of 10µM and immediately added to cells for 10minutes. Thereafter, PIP3
583 was removed and fresh medium and additional Torin1 was added for further 2hrs. The control
584 sample was treated with DMSO as a vehicle control. Cells were fix and further process for
585 immunocytochemistry (ICC).

586

587 **Western Blot analysis and qPCR**

588 Around 10^4 freshly sorted NSCs and ENB cells were collected in PBS with 10% FBS on ice
589 for protein analysis by western blot. For re-probing, membrane stripping was performed
590 according to the protocol from Cell Signaling technologies. For primary cultures, cells were
591 collected, washed with PBS and lysed as described before.
592 The following primary antibodies were used for western blot analyses. Phos EGFR Tyr1068
593 (rabbit, 1:1000), EGFR (rabbit, 1:1000), phos S6 Ser240/244 (rabbit, 1:1000), S6 (rabbit,
594 1:10,000), phos p70 S6K Thr421/Ser424 (rabbit, 1:1000), p70 S6K (rabbit, 1:1000) and
595 Tuberin/TSC2 (rabbit, 1:1000) were from Cell Signaling Technologies; DUSP4 (rabbit,
596 1:800), RHEB (mouse, 1:1000), RPS20 (rabbit, 1:1000), Sox2 (rabbit, 1:1000), VASH2
597 (rabbit, 1:1000), vinculin (rabbit, 1:5000) were from Abcam; actin (rabbit, 1:1000) and

598 RPL22 (mouse, 1:1000) were from Santa Cruz; Sp8 (rabbit, 1:1000) was from Millipor; PLP1
599 (chicken, 1:400) was from Neuromics; anti-HA (mouse, 1:1000) was from BioLegend.
600 For qPCR analysis of mRNA abundance in freshly sorted NSCs and ENBs, we collected
601 around 5,000 cells of each type. For primary NSCs in culture, around 10^5 cells were used.
602 Total RNA was extracted with the Picopure RNA isolation kit (Thermo Fisher Scientific).
603 cDNA was synthesized using the SuperScript VILO kit (Thermo Fisher Scientific). qPCR
604 reactions were performed in three technical replicates with the Power SYBR™ Green PCR
605 Master Mix (Thermo Fisher Scientific) and QuantiTech primers specific for mouse genes
606 (Qiagen). Cycles of amplification were made in the CFX384 Real-Time System (Bio-Rad).
607 Excel (Microsoft) was used to analyse the qPCR data.
608
609 **Immunocytochemistry, immunohistochemistry and RNA *in situ* hybridization**
610 Cells were fixed for 20min at room temperature using 2% PFA in the medium. Staining was
611 performed using standard procedures with following antibodies: anti-Sox2 (mouse, Abcam,
612 1:500) and anti-pS6 Ser240/244 (rabbit, Cell Signaling, 1:1000). OPP visualization was done
613 after all staining steps. For this, the alkyne group of OPP was detected using an Alexa488- or
614 Alexa647-coupled azide according to the Click-iT Cell Reaction Buffer Kit (Life
615 Technologies).
616 For tissue staining, mice were transcardially perfused first with HBSS and then with 4% PFA,
617 following overnight postfixation. Vibratome sections of 50-70µm were prepared for tissue
618 staining only, for RNA *in situ* hybridization cryosections of 11-13µm were prepared.
619 Following antibodies were used for ICC/IHC: anti-DCX (goat, Santa Cruz, 1:500), anti-DCX
620 (guinea-pig, Merck Millipore, 1:1000), anti-pS6 Ser240/244 (rabbit, Cell Signaling, 1:1000),
621 anti-NeuN (mouse, Merck Millipore, 1:500), anti-pH3 (mouse, Merck Millipore, 1:500), anti-
622 GFAP (mouse, Merck Millipore, 1:1000), anti-GFAP (rabbit, Merck Millipore, 1:1000), anti-
623 HA (mouse, Covance, 1:1000), anti-GFP (chicken, Aves, 1:1000), anti-RFP (rabbit,
624 Rockland, 1:1000), anti-Sox2 (goat, Santa Cruz, 1:500), anti-Sox2 (rabbit, Abcam,

625 1:1000),anti-Calretinin (rabbit, Merck Millipore, 1:1000), anti-GLAST (guinea pig, Frontier,
626 1:1000), anti-Mash1 (rat, RDI Fitzgerald, 1:500).
627 RNA *in situ* hybridization was performed using RNASCOPE Multiplex Fluorescent Assay
628 (Advanced Cell Diagnostics) with one major modification of the protocol: To allow
629 subsequent protein staining we skipped pretreatment steps as it is described in the
630 manufacturer's protocol and instead only did extended (15min, 95°C) heat-based target
631 retrieval using a modified citrate buffer (Target Retrieval Solution, Dako). Additional
632 immunofluourescence was done following the mRNA detection following standard
633 procedures.
634
635 **Polysome fractionation and protein/RNA isolation**
636 Polysome fractionation for cultured cells with subsequent protein and/or RNA isolation was
637 performed essentially following a previously published protocol for CNS tissue leaving out
638 initial steps of tissue preparation[46]. Cells were acutely treated for 5 min with cycloheximide
639 in culture medium (100µg/mL) and subsequently collected, washed in PBS/CHX and lysed in
640 polysome lysis buffer (PLB, 20 mM Tris HCl, pH 7.4, 5 mM $MgCl_2$, 120 mM KCl, 1%
641 Nonidet NP40, 100µg/mL CHX, 1x Roche complete protease inhibitor, 200 U/mL RNAsin
642 from Promega, 14 mM b-mercaptoethanol). Lysates were centrifuged and the supernatant was
643 added on sucrose gradients (17.5-50%). Samples were centrifuged for 2.5 hours at 35.000rpm
644 at 4°C in an ultracentrifuge (Beckman L8M). Samples were fractionated in 12 fractions
645 containing one mL sample using an Isco fractionator while monitoring absorption at 254nm
646 wavelength. RNA isolation was performed using acidic Phenol-Chloroform-Isoamylalcohol
647 (PCI, 25:24:1, Thermo Fisher Scientific). Alternatively, proteins were precipitated using
648 trichloroacetic acid (TCA).
649
650 **Imaging**
651 Confocal images were acquired using a Leica TCS SP5 confocal microscope. Image J was
652 used for processing and images were only adjusted for brightness and contrast. For OPP

653 quantifications, all images within compared groups were acquired with identical settings.
654 Analysis was performed in ImageJ software using a custom-written macro for unbiased
655 segmentation and quantification of pixel intensity and cell size. OPP quantifications are
656 depicted as the integrated pixel intensity within a cell and normalized to a reference group
657 within the same experiment. In graphs, mean and SD are shown. Illustrator CS5 (Adobe) was
658 used for figure assembly.
659
660 **Processing and analysis of RNAseq and RIBOseq data**
661 Sequence reads from both RNAseq and RIBOseq samples were aligned to the mouse
662 reference genome (ENSEMBL Release 80) and the ENSEMBL gene annotation (Release 80)
663 using the STAR alignment algorithm version 020201[47] with the proposed the ENCODE
664 settings to generate gene-specific raw count values. Expected gene counts and TPM values
665 (transcripts per million) were computed using RSEM (version 1.2.21)[48] with bowtie2 (version
666 2.2.6) with the same genome and verison and annotation. Differential gene expression
667 analysis between developmental stages of the RNAseq data was conducted by the
668 R/Bioconductor package DESeq2[49]. Thereby p-values were computed by fitting a negative
669 binomial distribution and subsequent testing by a Wald test. P-values were corrected for
670 multiple testing by controlling the false discovery rate applying the method of Benjamini-
671 Hochberg. For RIBOseq data the same analysis was applied to analyze the differential
672 abundance of ribosome bound RNA.
673 To assess the translation efficiency, genes with an average log2 read count of at least 10 were
674 considered. At first, a linear model was fitted for each replicate individually to explain the
675 RIBOseq data by a linear combination of RNAseq data (representing efficient translation) and
676 RIBO- (representing tissue background expression). Analysis of variance of this part provides
677 the proportion of variance that is explained by RNAseq and by RIBO- in each replicate
678 separately. The RIBOseq signal that cannot be explained by RNAseq or RIBO- can be
679 explained by either enhanced or repressed translation. To assess, if the detected enhanced or
680 repressed translation was statistically significant, we compared the two replicates and test, if

681 the remaining signal is different from zero by applying a moderated t-test implemented in the
682 R/Bioconductor package limma[50]. P-values were corrected for multiple testing by the method
683 of Benjamini-Hochberg. At this stage the analysis of variance provides the proportion of
684 variance that can be explained by translation efficiency (correlated signal) and the remaining
685 unexplained variance (uncorrelated signal) that is most likely of technical source. Full
686 documentation of computational analysis can be found as a supplementary document.
687
688 ***De novo* motif analysis**
689 3' UTR, 5'UTR and protein coding sequences of all protein coding genes were tiled in 6-mer
690 nucleotide sequences. For each developmental stage separately, for translationally repressed
691 and enhanced genes separately, and for 3'UTR, 5'UTR and coding sequence separately, an
692 unbiased motif analysis was performed. For each possible 6-mer, the number of genes
693 containing the tested 6-mer in the set of repressed (enhanced) genes and in the remaining
694 genes was computed. A p-value was computed by a binomial test and corrected by the
695 method of Benjamini-Hochberg. All over- or underrepresented motifs at a false discovery rate
696 of 10% were reported (Supplementary Table 5).
697
698
699
700
701

Main Figure Legends

Figure 1 Global protein synthesis is highly dynamic during neurogenesis. a, Sorting strategy for different stages of NSC differentiation. **b,** Representative images of OPP incorporation with specific marker expression, GLAST for NSCs, DCX for neuroblasts. **c,** Quantification of OPP incorporation relative to qNSCs. **d,** Strategy to compare protein synthesis of olfactory bulb neuroblasts (LNB; $DCX^{+}NeuN^{-}$) to early neurons (EN; $DCX^{+}NeuN^{+}$) and mature neurons ($DCX^{-}NeuN^{+}$). **e,** Representative images of OPP incorporation of LNBs, ENs and mature neurons. **f,** Quantification of OPP incorporation of LNBs, ENs and neurons (relative to neurons). qNSC: quiescent NSC, aNSC: active NSC, NP: neurogenic progenitor, ENB: early neuroblast (SVZ), LNB: late neuroblast (OB), EN: early neuron, OPP: O-Propargyl-puromycin. Statistical significance by student's t-test (Mann-Whitney). All scale bars: 10µm.

Figure 2 RiboTag mouse models target stages of neuronal differentiation. a, Schematic representation of RiboTag mouse lines used for the study, HA-tag allows isolation of ribosome-associated mRNA, cell sorting based on eYFP expression alllows isolation of total mRNA. **b,** IHC confirming HA-tag expression in NSCs (controlled by the Tlx-promotor) of the SVZ, labeled cells are mostly $GFAP^{+}pH3^{-}$. Quantification shows that labeled cells in the TiCRY-SVZ are mostly NSCs ($eYFP^{+}/DCX^{-}$: 88.32%±1.8), some ENBs ($eYFP^{+}/DCX^{+}$: 7.75%±1.9) and few of unknown identity further away from the ventricle ($eYFP^{+}/DCX^{-}$: 3.94%±1.3) at the timepoint of the experiments (4dpi). n=3. Scale bars: 50µm. **c,** IHC confirming expression of HA-tag in migrating neuroblasts (controlled by the Dcx-promotor) both in the SVZ/RMS (ENB) as well as in the OB (LNB). Quantification shows that labeled cells within the DiCRY-SVZ are mostly ENBs ($eYFP^{+}/DCX^{+}$: 90.52%±1.3) and some DCX negative cells of unknown identity ($eYFP^{+}/DCX^{-}$: 9.49%±1.3). DiCRY-olfactory bulb labeled-cells could be detected in all layers (GCL/MCL: 70.33%±1.3, EPL: 4.25%±0.3, PGL: 23,60%±1) indicating no labeling bias. eYFP cells in the GCL/MCL were mostly LNBs ($eYFP^{+}/DCX^{+}$: 47.83%±2), few early neurons ($eYFP^{+}/DCX^{+}/NeuN^{+}$: 3.4%±0.9), some

neurons (eYFP$^+$/DCX$^-$/NeuN$^+$: 13%±2.9) and some cells of unknown identity (eYFP$^+$/DCX$^-$/NeuN$^-$: 6.1%±0.5), which most likey consisted of NeuN-negative subtypes of neurons as assessed by morphology and position. Few labeled-cells could be found in the EPL. These were mostly NeuN- negative neurons (eYFP$^+$/DCX$^-$/NeuN$^-$: 3.33%±0.1), few LNBs (eYFP$^+$/DCX$^+$/NeuN$^-$: 0.21%±0.1) and rarely NeuN-positive neurons (eYFP$^+$/DCX$^-$/NeuN$^+$: 0.03%±0.06). YFP-cells in the PGL were mostly LNBs (eYFP$^+$/DCX$^+$/NeuN$^-$: 22.4%±1), some early neurons (eYFP$^+$/DCX$^+$/NeuN$^+$: 1%±0.9) and rarely mature neurons (eYFP$^+$/DCX$^-$/NeuN$^+$: 0.2%±0.2). n=3. Scale bars: 100µm. **d,** IHC confirming expression of HA-tag in NeuN$^+$ neurons four weeks after initial labeling as DCX$^+$ neuroblasts. NeuN$^-$ cells in EPL and GL display mostly neuronal morphology. Most eYFP$^+$-cells lost DCX expression indicating their progression to a more differentiated stage. GCL/MCL cells were mostly mature NeuN$^+$-neurons (eYFP$^+$/DCX$^-$/NeuN$^+$: 67.7%±2) or NeuN$^-$-neurons (eYFP$^+$/DCX$^-$/NeuN$^-$: 7%±1.7). Again, only few cells could be found in the EPL with similar characteristics compared to the three days timepoint (mostly eYFP$^+$/DCX$^-$/NeuN$^-$: 3.1%±0.4). PGL cells were almost exclusively mature neurons (eYFP$^+$/DCX$^-$/NeuN$^+$: 20%±2.5). n=3. Scale bars: 100µm. All quantifications are based on IHC depicted in Extended Data Figure 2. RMS: rostral migratory stream, dpi/wpi: days/weeks post induction, GCL: granular cell layer, MCL: mitral cell layer, EPL: external plexiform layer, PGL: periglomerular layer.

Figure 3 RiboTag system allows parallel study of transcriptome and translatome. a, Expression of stage-specific marker genes for SVZ populations at the level of transcriptome (top) and translatome (bottom). **b,** Expression of stage-specific marker genes for OB populations at the level of transcriptome (top) and translatome (bottom). Expression values based on tags per million (TPM) reads after Trimmed Mean of M-values (TMM) normalisation. Black bars in RIBOseq base on mock immunoprecipitation using Cre- mice (no HA-tag expression, RIBO-) representing average expression in the respective tissue corresponding to background binding (=noise). **c-e,** Overlap of differential expressed genes between RNAseq and RIBOseq for transition of NSC to ENB (c), ENB to LNB (d) and LNB

to NEURON (e, FDR=10%). Only protein coding genes are considered. Gene set enrichment analysis on shared genes (marked in red) confirms enrichment of stage specific gene ontologies.

Figure 4 Stage-specific repression and enhancement of transcripts. a, Scheme describing the three datasets, which are implemented into analysis of translation efficiency. RIBO-sample resembles mock immunoprecipitation with HA-tag negative mice to assess background binding. **b,** Summary of the fraction of genes, which are repressed or enhanced in each population (only protein coding, >1000 reads). Few transcripts showed repression (32/4500, p=0.1) or enhancement (9/4500, p=0.1) in NSCs. ENBs feature a higher fraction of genes that were translationally repressed (282/3445, p=0.1) or enhanced (63/3445, p=0.1). LNBs displayed higher divergence of transcriptome and translatome (Repressed: n=622/1958, p=0.1; Enhanced: n=225/1958, p=0.1). Neurons showed the highest degree of variation between RNAseq and RIBOseq. Most of the analyzed genes showed repression (n=714/1443, p=0.1) or enhancement (n=214/1443, p=0.1). **c,** Scatter plots for each population showing translation efficiency. Grey dots: genes with linear ratio between transcript abundance (RNA) and translation (RIBO), blue dots: genes which are translationally repressed (dark: 1% FDR, light: 10% FDR), red dots: genes with enhanced translation (red: 1% FDR, orange: 10% FDR). Increasing number of genes with enhanced or repressed translation with further differentiation. **d,** Matched plots to the order of scatter plots in (b) illustrating temporal changes in translation efficiency of genes being significantly repressed or enhanced in the respective population. Only highly significant genes marked here in color (FDR=1%), Sox2 marked in black as an example for genes that are translationally repressed at the ENB stage. **e,** Matched plots to the order of scatter plots in (b) illustrating temporal changes in transcript abundance of genes being significantly repressed or enhanced in the respective population. Only highly significant genes marked here in color (FDR=1%), Sox2 marked in black as an example for genes that are translationally repressed at the ENB stage. **f,** Comparison of

repressed- and enhanced genes over stages reveals increasing overlap with progression of cells. LNBs and neurons feature high overlap of repressed genes (n=311).

Figure 5 Sox2 is post-transcriptionally repressed in ENBs and expressed at high levels in a subpopulation of olfactory bulb interneurons. a, Sox2 locus in the integrated genome viewer (IGV) both of total RNA (T) and ribosome-bound RNA (R) for populations of interest, histogram shows abundance of reads. Different color hues mark biological replicates. Black histogram indicates background binding (RIBO-). Sox2 shows no ribosome binding specifically at ENB stage indicating post-transcriptional repression. **b,** Representative image for parallel *in situ* hybridization and immunohistochemistry for Sox2 protein/RNA in NSCs (marked by Tlx-TOMATO) and ENBs (marked by DCX) validating Sox2 repression event. Scale bar: 10µm. **c,** Quantification or Sox2 RNA (molecules per cell) and protein expression (total fluorescence) by manual segmentation. Regression line indicates different translation efficiency. Quantified 144 NSCs and 145 ENBs from two mice. **d,** Ratio of protein expression to RNA abundance indicates greatly reduced translation efficiency of SOX2 in ENBs. Significance by students t-test (Mann-Whitney). **e**, Sox2 protein and mRNA abundance in freshly sorted NSCs and ENBs. Protein levels were analyzed by WB (representative WB, upper panel) and the mRNA was quantified by qPCR (lower panel). Vinculin served as a loading control. The fold change was calculated based on three technical replicates. **f,** Staining of olfactory bulb periglomerular layer showing Dcx-eYFP traced cells (4wpi) which coexpress SOX2 and the neuronal marker Calretinin. Scale bar: 50µm. **g,** Comparison of short (3dpi) and long (4wpi) tracing of Dcx-eYFP cells shows increase of $eYFP^{+}SOX2^{+}$ cells with time indicating contribution of migrating, newborn neurons to the pool of $SOX2^{+}$ neurons in the periglomerular layer. Scale bar: 50µm.

Figure 6 Pyrimidine-rich motifs (PRMs) in the 5' UTR predict translational repression under mTORC1 mediated global arrest a, Motif analysis reveals enrichment of pyrimidine-rich motif (PRM) CTCTT in the 5' untranslated region (UTR) of genes, which are

repressed at the ENB stage. **b,** Relation of the presence of a 5' PRM and a drop in translation efficiency at the ENB or LNB stage indicates stage-specific repression of 5' PRM containing transcripts in ENBs independent of the total number of repressed genes (1% FDR). **c,** Staining for phosphorylation of ribosomal protein S6 (pS6) in the SVZ as readout for mTORC1 activity. Comparison of NSCs (Tlx-eYFP^{+}) and ENBs (DCX^{+}). All ENBs show low levels of pS6 (green arrow), while some NSCs show high pS6 (orange arrows) and others show low levels of pS6 (yellow arrow). Scale bar: 50µm. d, WB analysis of the steady-state level of a number of proteins involved in mTOR signaling in NSCs and ENBs freshly sorted from the SVZ. Vinculin served as a loading control. **e,** Freshly isolated ENBs were directly fix or exposed to PIP3 alone or with Torin and the levels of pS6 and Sox2 assessed by ICC. NSCs were directly fix after isolation and stained by ICC. Representative images of Sox2 (red) and pS6 (turquoise) in the different groups are shown (left panel). Scale bar: 5µm. The relative expression of Sox2 and pS6 in the different groups is shown in right panel. Statistical significance was calculated by students t-test $p < 0.01^{**}$, $p < 0.005^{***}$.

Extended Data Figure Legends

Extended Data Figure 1

a, FACS gates for NSCs labeled by Tlx-TOMATO four days post induction. NSCs, which are labeled by recombination under the Tlx-promoter, contain both quiescent ($GLAST^+EGFR^-$) and active NSCs ($GLAST^+EGFR^+$). Prom1 was not used in this experiment since it is known that Tlx does not recombine in astrocytes. **b,** Composition of $TOMATO^+$ cells four days after induction. 52.1%±0.6 are NSCs ($GLAST^+$) while 45.6%±0.3 are non-NSCs ($GLAST^-$). The numbers do not sum up to 100% since some few cells lay between gates. NSCs contain 51.7%±9.1 quiescent NSCs ($EGFR^-$) and 46.7%±9.1 active NSCs ($EGFR^+$). $GLAST^-$ cells contain 62.7%±1.6 neurogenic progenitors (NPs, $EGFR^+PSA\text{-}NCAM^-$) and 33.3%±2 neuroblasts ($EGFR^-PSA\text{-}NCAM^+$). **c,** Quantification of OPP incorporation in lineage-traced NSCs and ENBs relative to ENBs. $p < 0.0001^{****}$.

Extended Data Figure 2

a, Top: NSCs isolated from TiCRY mice express HA-tag, replicates show different levels indicating variability based on induction efficiency. Cells of WT mice do not express HA-tag. Bottom: HA-tag is associated to RPL22 since staining shows characteristic 8kDa shift due to HA-tag (23kDa instead of 15kDa). Isolated TiCRY cells entirely replaced WT-RPL22 by RPL22-HA. **b,** Representative Bioanalyzer profiles showing that input RNA levels do not vary between Cre^+ TiCRY mice (expressing HA-tag) and Cre^- TiCRY mice (no HA-tag), however samples from Cre^+ mice reveal approximately 3-fold more RNA over the background level of Cre^- mice after HA-immunoprecipitation. **c,** Enrichment of cell type specific transcripts by qPCR after HA-immunoprecipitation. Efficiency by enrichment of immunoprecipitation- over input samples. Comparison of NSCs from TiCRY mice homozygous for the Rpl22-tag (p/p), heterozygous for the Rpl22-tag (p/+) and WT mice indicates linear relationship between HA-tag expression and immunoprecipitation efficiency. NeuN serves as negative control. Cells isolated from NiCRY mice (Nes-inducible-Cre-Rpl22.HA-eYFP). **d,** OPP incorporation does not vary between HA-tag expressing- and non-expressing cells indicating no major impact on global protein synthesis. NSCs isolated from NiCRY mice. Scale bar: 10µm. n= 30 cells each. **e,** Polysome fractionation using cultured NSCs indicates efficient incorporation of RPL22-HA (antibody against HA-tag) into actively translating polysomes (see fractions 8-12). Total lysate resembles positive control (+ctr). Cells from TiCRY mice. **f,** Disruption of polysomes using EDTA leads to shift of RPL22-HA

expression to light fractions indicating specific association to active ribosomes. **g-j,** Immunofluorescence estimating cell type composition based on eYFP expression and characterisitic marker protein expression, see quantification in main figure, all scale bars: 50µm: NSCs using TiCRY mice 4dpi (g), green arrow indicating NSCs, yellow arrows indicating ENB contamination, white arrow showing rare labeled cells outside the SVZ. ENBs using SVZ of DiCRY mice 3dpi (h), yellow arrows pointing at ENBs and white arrow showing rare labeled cells outside the SVZ. LNBs using OB of DiCRY mice 3dpi (i), labeled cells are mostly in the core of OB expressing DCX protein. Neurons using OB of DiCRY mice 4wpi (j), labeled cells throughout the OB mostly coexpressing NeuN protein. **k,** Time course of development of labeled cells in TiCRY mice.

Extended Data Figure 3

a, Enrichment of cell type specific transcripts for NSC, ENB, LNB and Neuron by fold enrichment of HA-IP RNA (RIBO) of Cre^+ mice over Cre^- mice, assessed by qPCR. Genes expected to be strongly enriched after successful immunoprecipitation are labeled in red. **b,** FACS sorting strategy for isolation of NSCs and ENBs based on eYFP expression. eYFP negative cells were collected and used as control samples for enrichment analysis. **c,** Enrichment of cell type specific transcripts by comparison of $eYFP^+$ and $eYFP^-$ cells by qPCR. Genes expected to be strongly enriched after correct enrichment are labeled in red. All samples were assessed by qPCR before submission for sequencing. **d,** Differential gene expression based on RNAseq. Subsequent populations were compared and significantly changing genes marked in red (FDR: 10%). **e,** Differential gene expression based on RIBOseq without normalization for RIBO-. Subsequent populations were compared and significantly changing genes marked in red (FDR: 10%).

Extended Data Figure 4

a, Summary of the absolute number of genes, which are repressed or enhanced in each population (only protein coding). **b,** Analysis of explained variance scoring the contribution of background (RIBO-), total RNA (RNAseq), translation efficiency (RIBOseq over RNAseq

and RIBO-) and unknown residual noise to the RIBOseq data of each population. **c,** As in (b), but comparing only the proportion of variance explained by translation efficiency and RNA. Translation efficiency explains more of the data in neurons compared to earlier developmental stages and NSCs indicating increased importance of translational regulation in neurons. **d**, Correlation in mRNA abundance between the data derived from RNAseq (upper panel) and quantified by qPCR (lower panel) of candidate genes with different translation efficiency upon the NSC-to-ENB transition. The right panel presents a correlation plot for fold changes measured by both approaches. **e**, Fold changes in the RIBOseq fraction of the genes analyzed in (f). **f**, Representative WB image showing relative abundance in freshly sorted NSCs and ENBs of some proteins whose genes change their translation efficiency upon the NSC-to-ENB transition. Vinculin serves as loading control.

Extended Data Figure 5

a, Representative images for parallel *in situ* hybridization (ISH) and immunocytochemistry of freshly sorted cells of the SVZ. Comparison of NSCs ($GLAST^{+}PROM^{+}$), neurogenic progenitors (NPs, $GLAST^{-}PROM^{-}EGFR^{+}$) and ENBs ($GLAST^{-}PROM^{-}PSA\text{-}NCAM^{+}$). Stained for cell type specific marker proteins and Sox2 protein. ISH for Sox2 mRNA. Scale bar: 5µm. **b,** Quantification of SOX2 protein and RNA expression in NSCs (n=22), NPs (n=49) and ENBs (n=35). Regression line indicates most efficient translation in NSCs. **c,** Ratio of protein expression to RNA abundance indicates higher translation efficiency of Sox2 in NSCs when compared to NPs or ENBs. Significance by students t-test (Mann-Whitney). **d,** Representative image for parallel *in situ* hybridization for Sox2 mRNA in NSCs (marked by Tlx-TOMATO) and ENBs (marked by DCX). Parallel detection of DapB (bacterial transcript) and Ppib (ubiquitous transcriptI) served as a negative- and positive control, respectively.
Scale bar: 10µm.

Extended Data Figure 6

a, Gene ontology analysis for genes either repressed (left panel) or upregulated (right panel) at the ENB stage. The repressed genes are mostly related to the protein synthesis machinery, whereas many upregulated genes are involved in development, differentiation and neuronal function. **b, WB of** Torin1-treated primary NSCs showing inhibition of p70 S6 kinase- and S6 phosphorylation, all indicators of mTORC1 activity. mTORC1 regulators TSC2 and RHEB, as well as Sox2, are not affected by 2h incubation with Torin1. Vinculin serves as loading control. **c,** WB of primary NSCs treated for 4h with erlotinib reveals a drop in EGFR phosphorylation accompanied by much lower levels of phospho p70 S6 kinase and phospho S6. TSC2, RHEB and Sox2, similar as for Torin1 treatment, remain at a constant level. **d,** Representative absorption profiles for vehicle- and Torin1-treated NSCs (2h) after sucrose gradient fractionation indicate slight repression in global translation upon torin1 treatment. Representative plots showing the distribution of mRNAs for some genes across the gradient fractions of the polysome profiles are shown. Note a strong shift of PRM+ mRNAs (Rpl18, Rps17, eIF3F, eEF1b2) but not PRM- (Sox9, Actin) to the fractions of light polysomes and non-translating complexes upon Torin1. Sox2 transcript distribution across the polysome fraction was not influenced following 2h Torin treatment **e,** Genes translationally upregulated upon the transition from NSCs to ENBs show slightly higher protein abundance (left panel; WB) but unaffected mRNA levels (right panel; qPCR) following 2h treatment with Torin1 in primary NSCs. **f,** Staining for phosphorylation of ribosomal protein S6 (pS6) in the OB as readout for mTORC1 activity. The core of the OB (marked with dashed line) which contains only LNBs (DCX^+) is enriched for high pS6, while only few neurons ($NeuN^+DCX^-$) have high levels of pS6. Scale bar: 50µm. **g,** Graphical abstract summarizing the findings of this study.

Figure 1

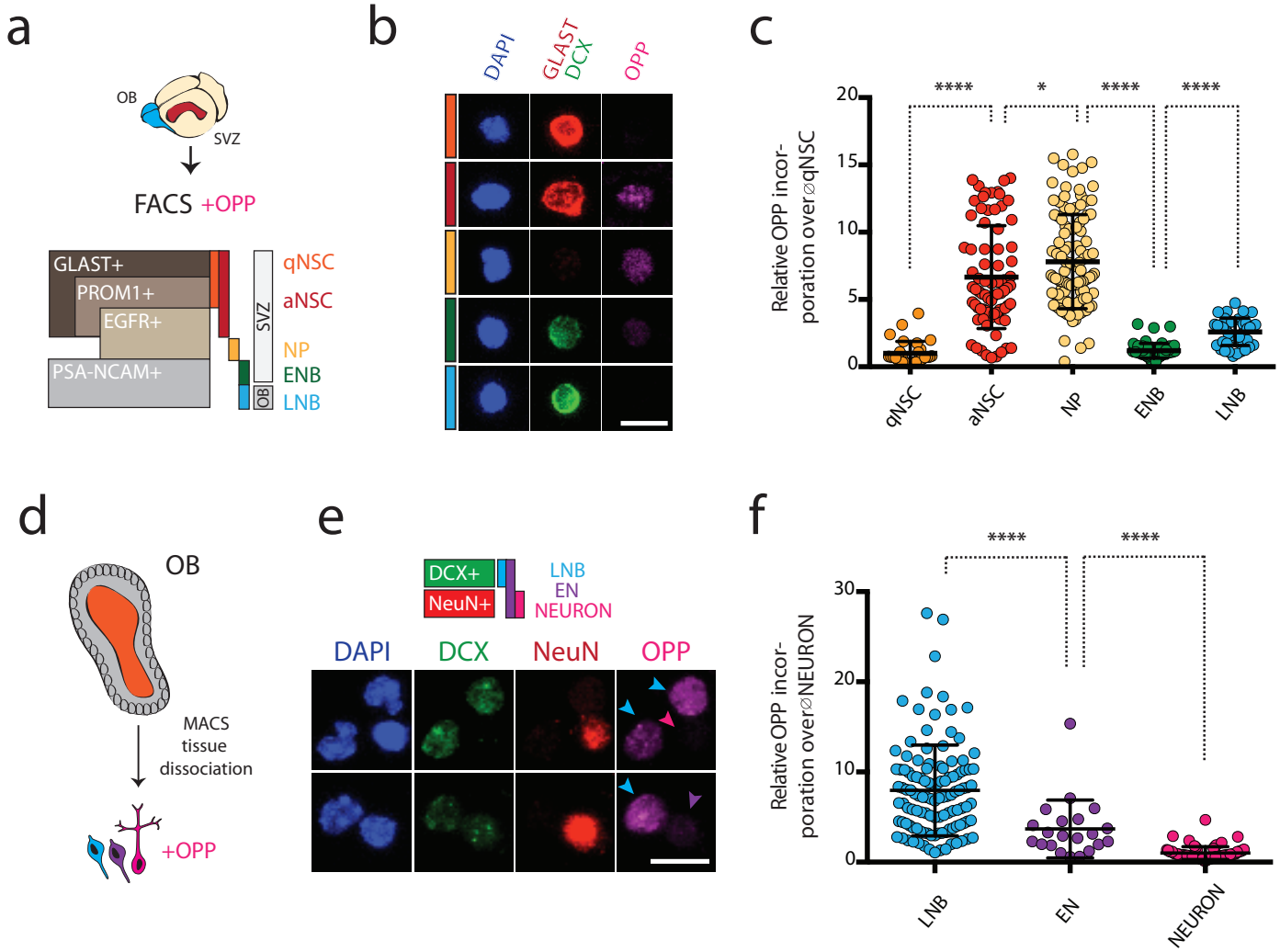
a
OB
SVZ
FACS +OPP
GLAST+
PROM1+
EGFR+
PSA-NCAM+
qNSC
aNSC
NP
ENB
LNB
SVZ
OB
b
DAPI
GLAST
DCX
OPP
c
Relative OPP incor-
poration over qNSC
20
15
10
5
0
****
*
****
****
qNSC
aNSC
NP
ENB
LNB
d
OB
MACS
tissue
dissociation
+OPP
e
DCX+
NeuN+
LNB
EN
NEURON
DAPI
DCX
NeuN
OPP
f
Relative OPP incor-
poration over NEURON
30
20
10
0
****
****
LNB
EN
NEURON

Figure 2

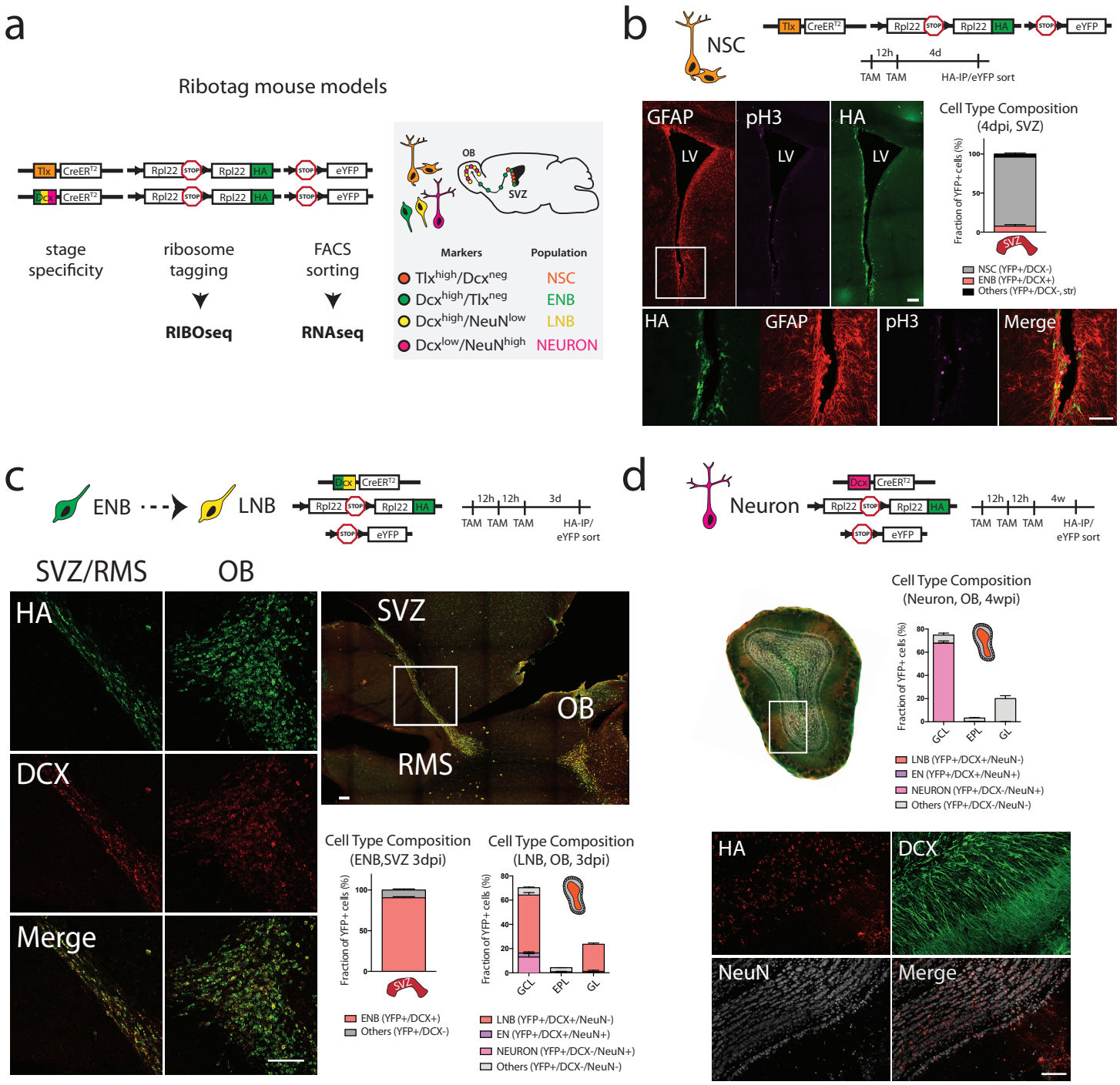
a
Ribotag mouse models
Tlx
CreER^{T2}
Dcx
Rpl22
STOP
HA
eYFP
stage specificity
ribosome tagging
FACS sorting
RIBOseq
RNAseq
OB
SVZ
Markers
Population
Tlx^{high}/Dcx^{neg} NSC
Dcx^{high}/Tlx^{neg} ENB
Dcx^{high}/NeuN^{low} LNB
Dcx^{low}/NeuN^{high} NEURON
b
NSC
12h
4d
TAM TAM
HA-IP/eYFP sort
GFAP
pH3
HA
LV
Merge
Cell Type Composition (4dpi, SVZ)
Fraction of YFP+ cells (%)
NSC (YFP+/DCX-)
ENB (YFP+/DCX+)
Others (YFP+/DCX-, str)
c
ENB
LNB
3d
TAM TAM TAM
SVZ/RMS
OB
DCX
RMS
Cell Type Composition (ENB,SVZ 3dpi)
Cell Type Composition (LNB, OB, 3dpi)
GCL
EPL
GL
ENB (YFP+/DCX+)
Others (YFP+/DCX-)
LNB (YFP+/DCX+/NeuN-)
EN (YFP+/DCX+/NeuN+)
NEURON (YFP+/DCX-/NeuN+)
Others (YFP+/DCX-/NeuN-)
d
Neuron
4w
Cell Type Composition (Neuron, OB, 4wpi)
NeuN

Figure 3

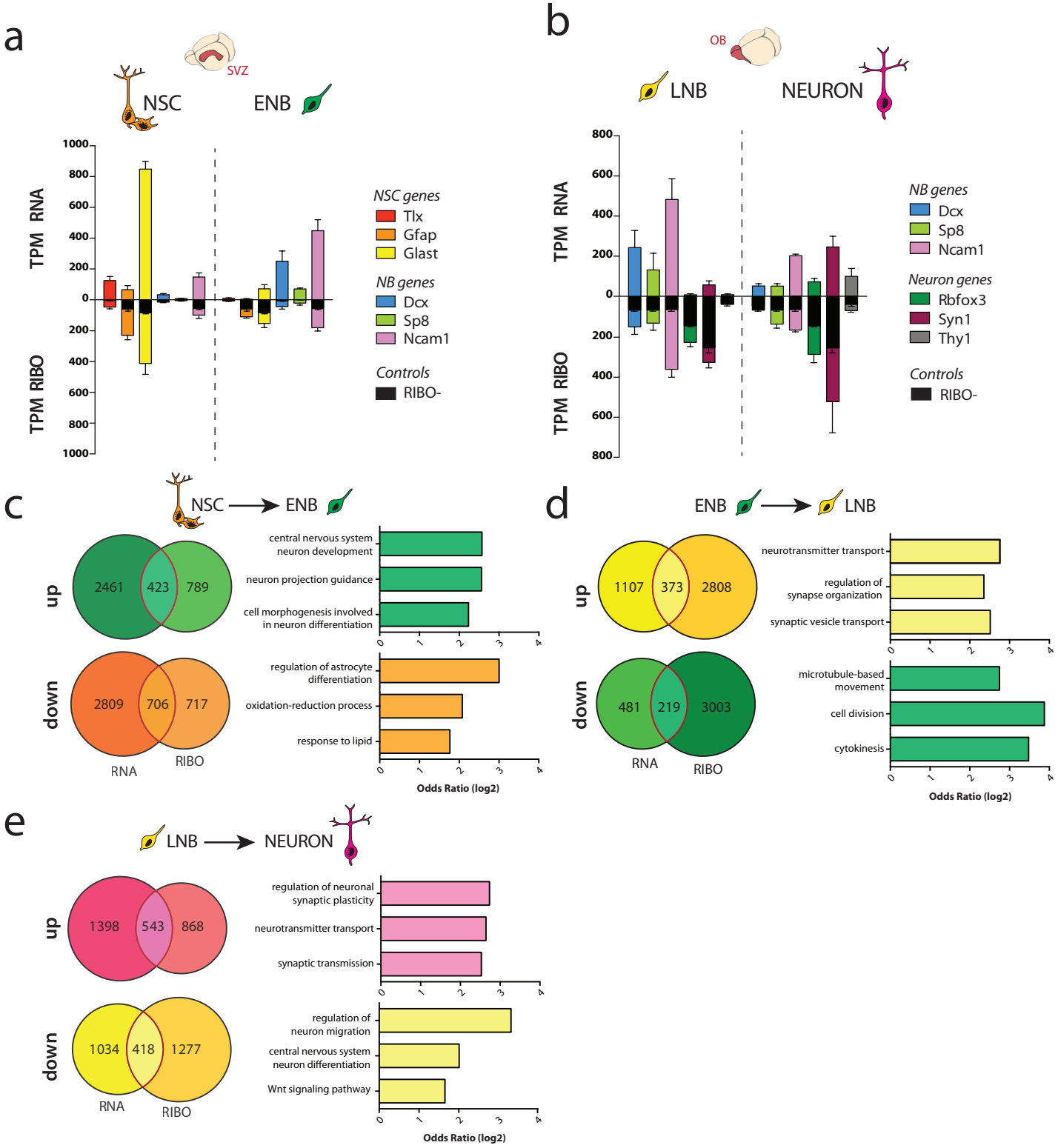
a
SVZ
NSC
ENB
TPM RNA
TPM RIBO
1000
800
600
400
200
0
NSC genes
Tlx
Gfap
Glast
NB genes
Dcx
Sp8
Ncam1
Controls
RIBO-
b
OB
LNB
NEURON
NB genes
Dcx
Sp8
Ncam1
Neuron genes
Rbfox3
Syn1
Thy1
Controls
RIBO-
c
NSC → ENB
up
down
2461
423
789
2809
706
717
RNA
RIBO
central nervous system neuron development
neuron projection guidance
cell morphogenesis involved in neuron differentiation
regulation of astrocyte differentiation
oxidation-reduction process
response to lipid
Odds Ratio (log2)
d
ENB → LNB
up
down
1107
373
2808
481
219
3003
RNA
RIBO
neurotransmitter transport
regulation of synapse organization
synaptic vesicle transport
microtubule-based movement
cell division
cytokinesis
Odds Ratio (log2)
e
LNB → NEURON
up
down
1398
543
868
1034
418
1277
RNA
RIBO
regulation of neuronal synaptic plasticity
neurotransmitter transport
synaptic transmission
regulation of neuron migration
central nervous system neuron differentiation
Wnt signaling pathway
Odds Ratio (log2)

Figure 4

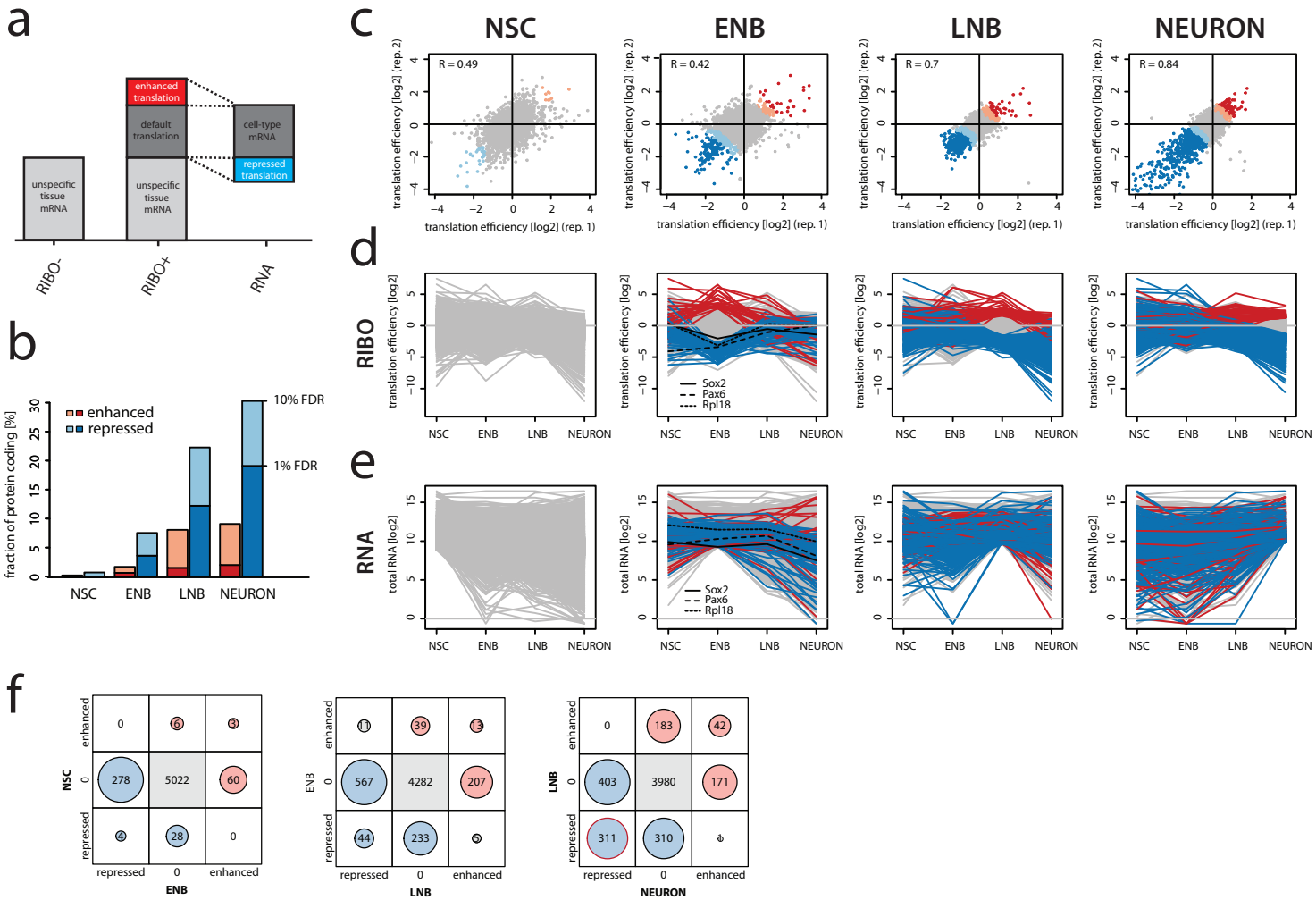
a
enhanced translation
default translation
cell-type mRNA
repressed translation
unspecific tissue mRNA
unspecific tissue mRNA
RIBO-
RIBO+
RNA
b
enhanced
repressed
10% FDR
1% FDR
fraction of protein coding [%]
NSC
ENB
LNB
NEURON
c
NSC
ENB
LNB
NEURON
R = 0.49
R = 0.42
R = 0.7
R = 0.84
translation efficiency [log2] (rep. 2)
translation efficiency [log2] (rep. 1)
d
RIBO
translation efficiency [log2]
Sox2
Pax6
Rpl18
e
RNA
total RNA [log2]
f
NSC
ENB
LNB
NEURON
enhanced
0
repressed
0
6
3
278
5022
60
4
28
0
11
39
13
567
4282
207
44
233
5
0
183
42
403
3980
171
311
310
6

Figure 5

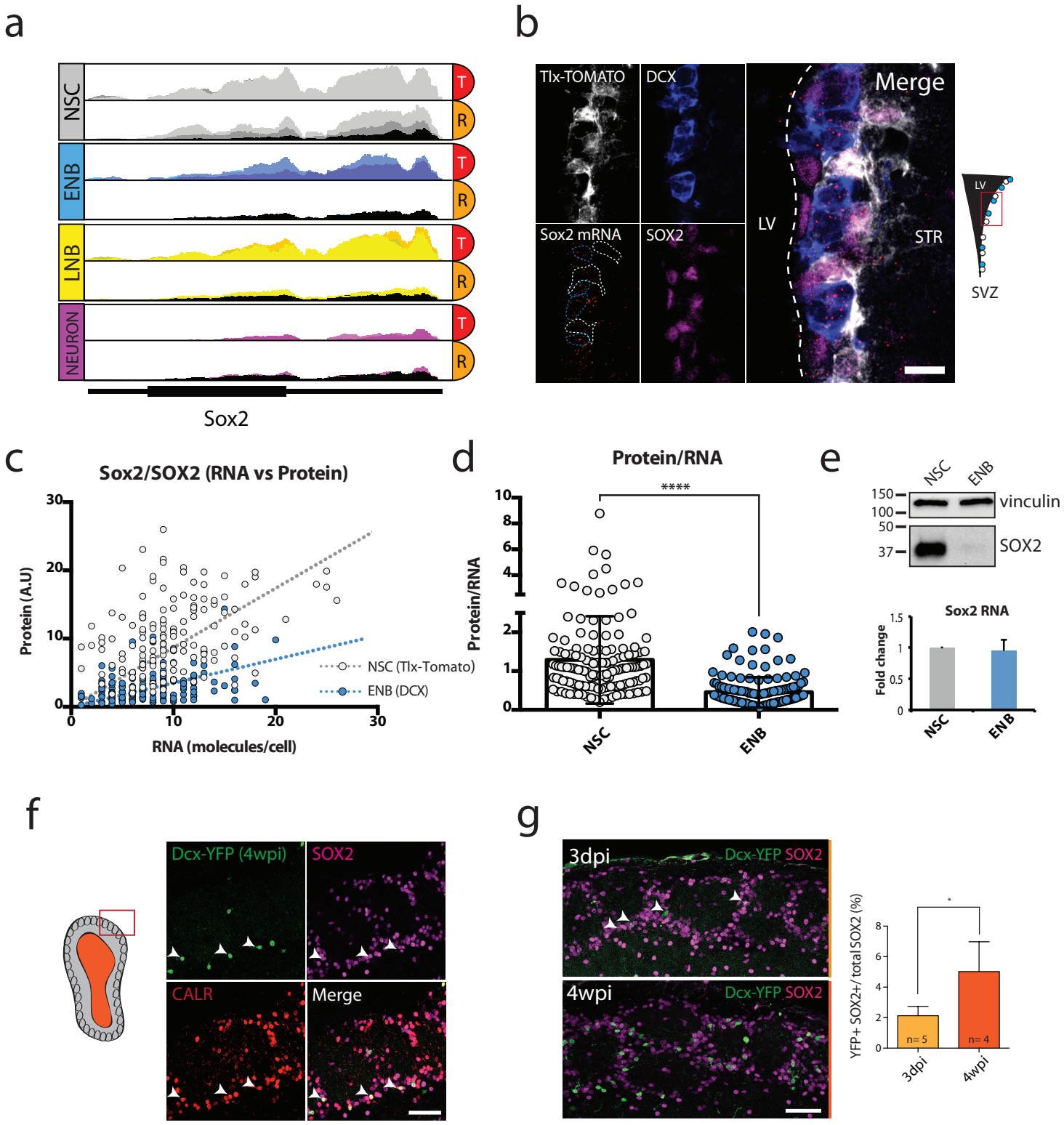
a
NSC
ENB
LNB
NEURON
T
R
Sox2
b
Tlx-TOMATO
DCX
Merge
Sox2 mRNA
SOX2
LV
STR
SVZ
c
Sox2/SOX2 (RNA vs Protein)
Protein (A.U)
RNA (molecules/cell)
NSC (Tlx-Tomato)
ENB (DCX)
d
Protein/RNA
****
Protein/RNA
NSC
ENB
e
NSC
ENB
150
100
50
37
vinculin
SOX2
Sox2 RNA
Fold change
NSC
ENB
f
Dcx-YFP (4wpi)
SOX2
CALR
Merge
g
3dpi
Dcx-YFP SOX2
4wpi
Dcx-YFP SOX2
YFP+ SOX2+/ total SOX2 (%)
n= 5
n= 4
3dpi
4wpi

Figure 6

a

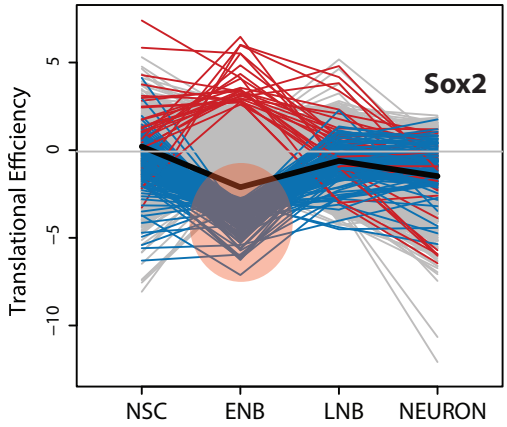

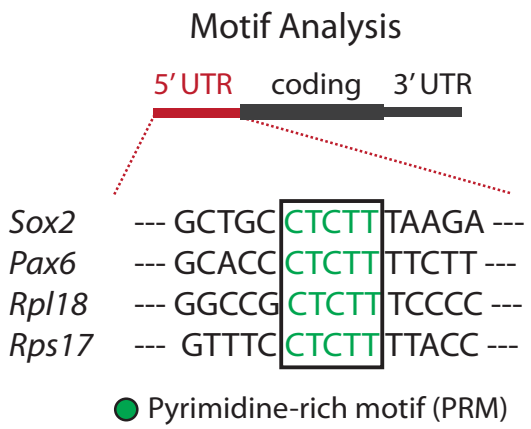

b

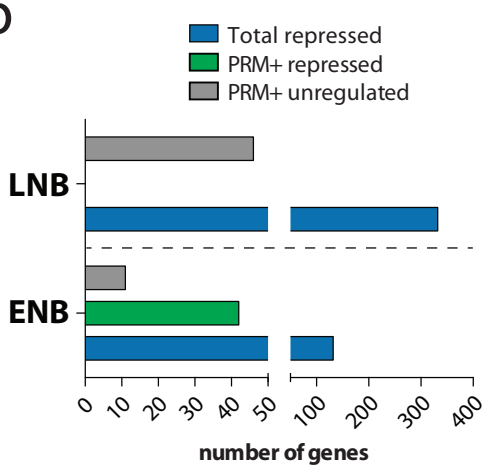

c

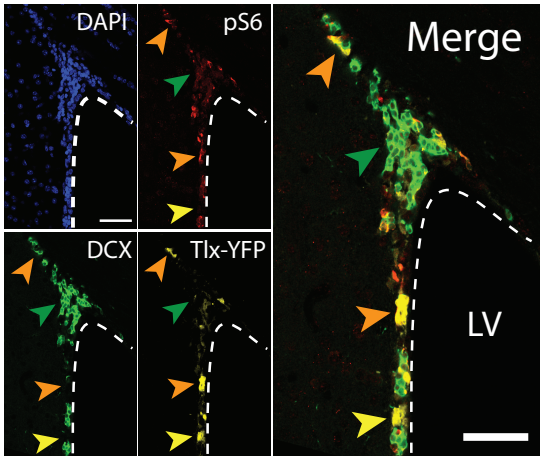

d

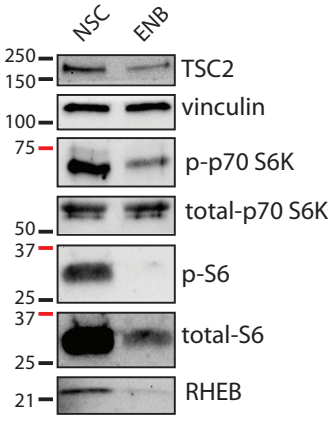

e

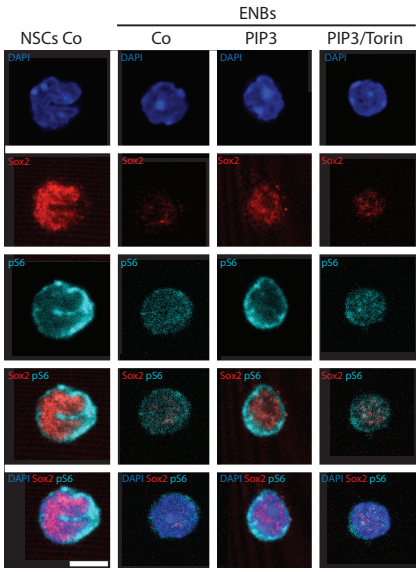

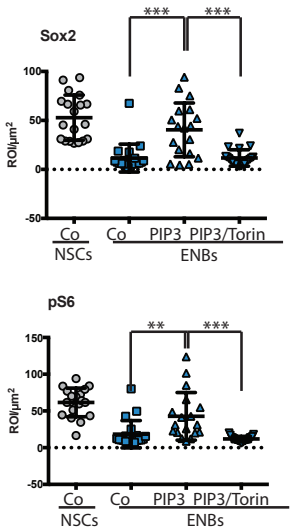

Extended Data Figure 1

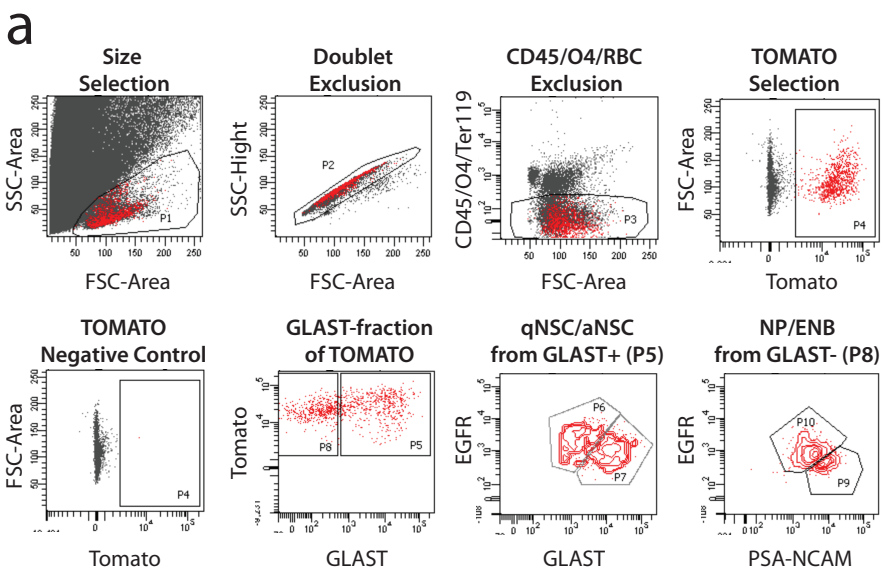

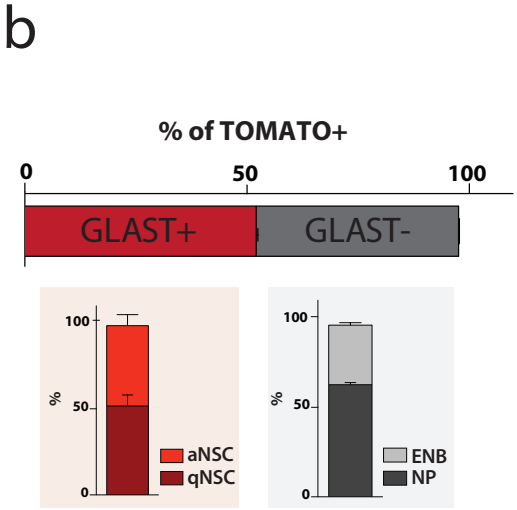

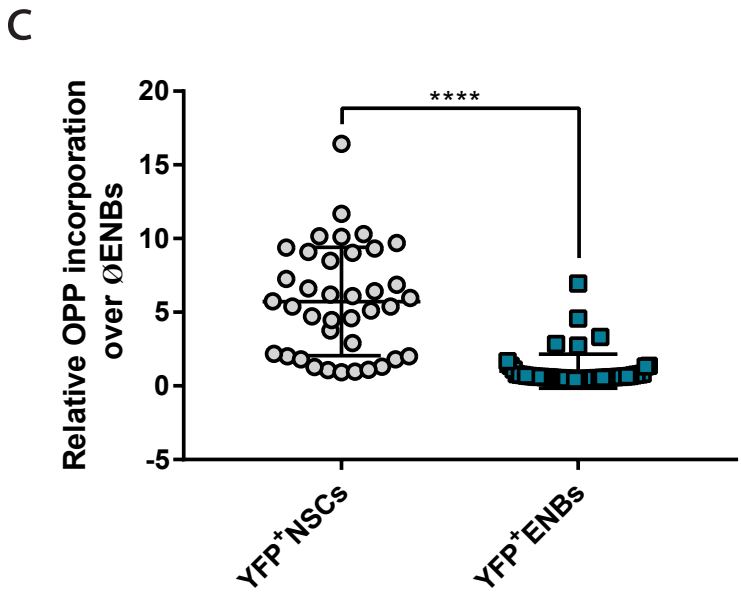

Extended Data Figure 2

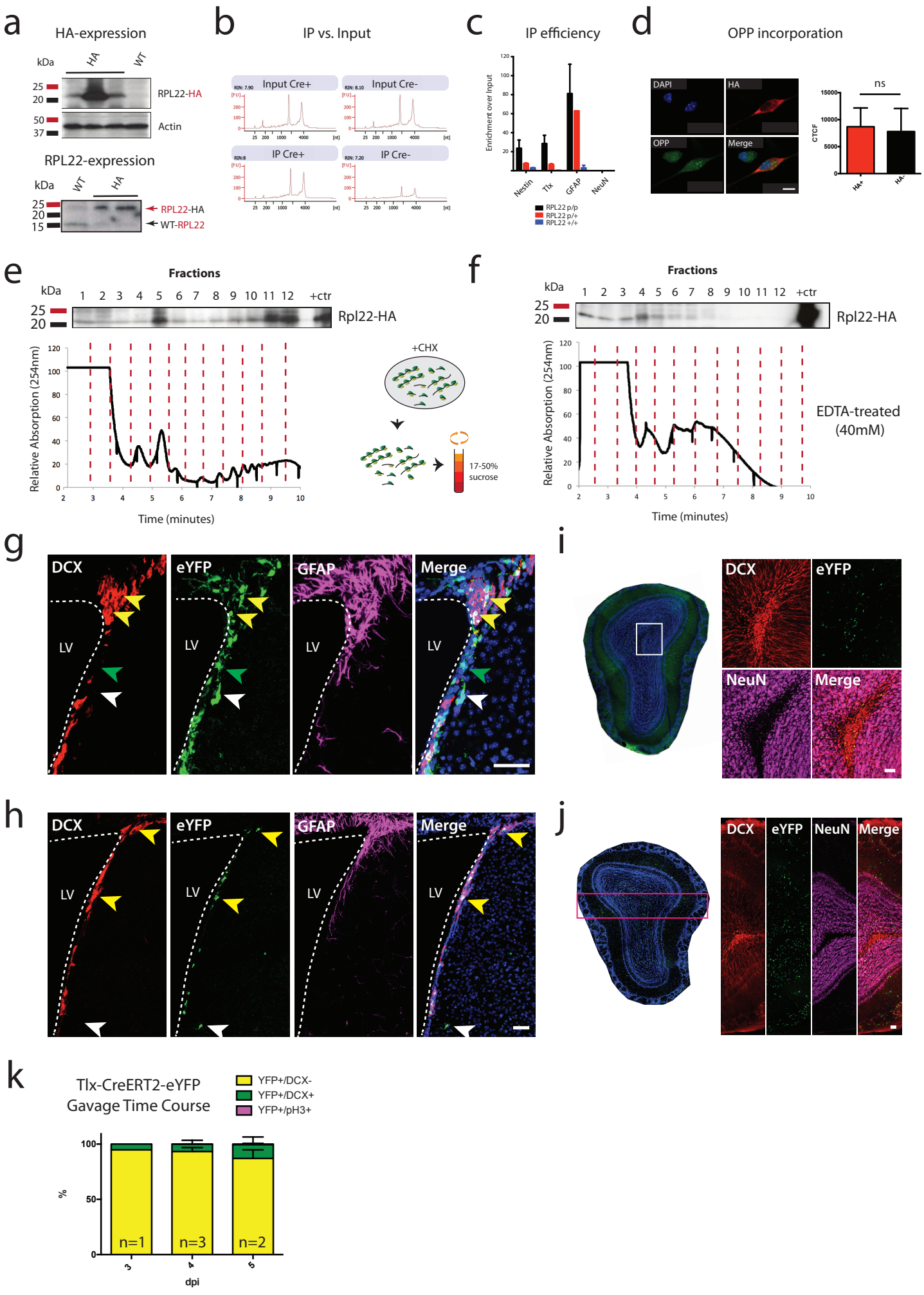

Extended Data Figure 3

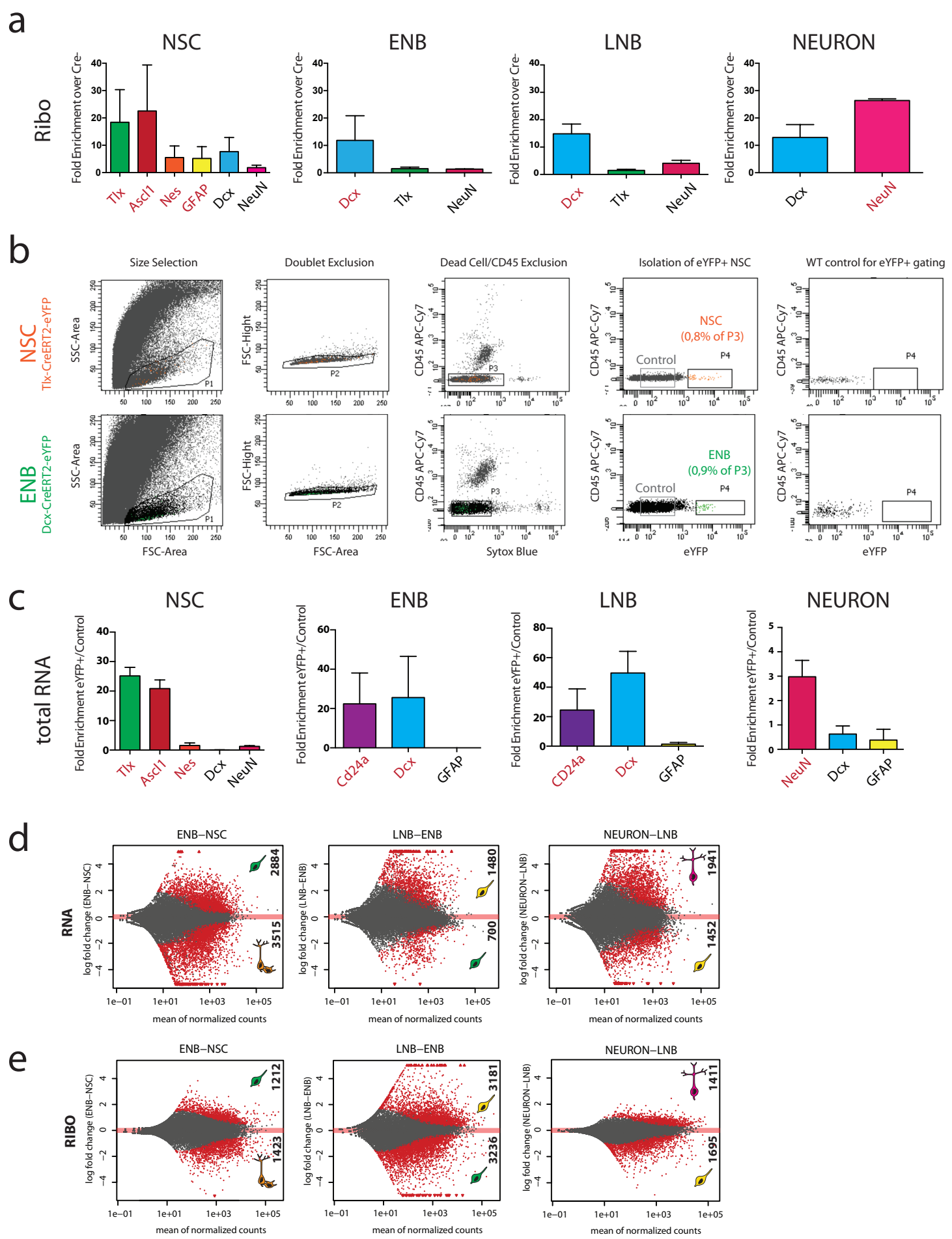

Extended Data Figure 4

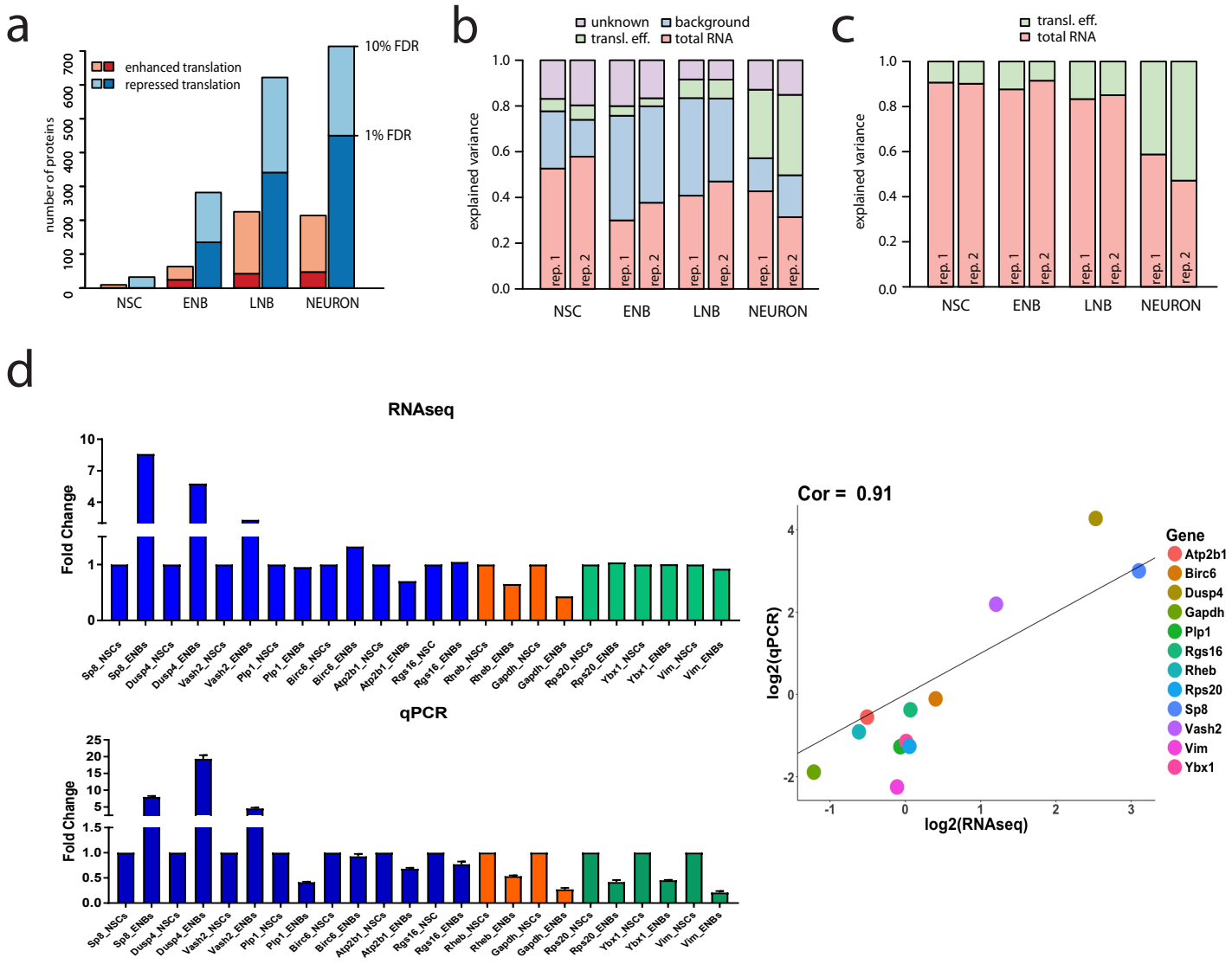

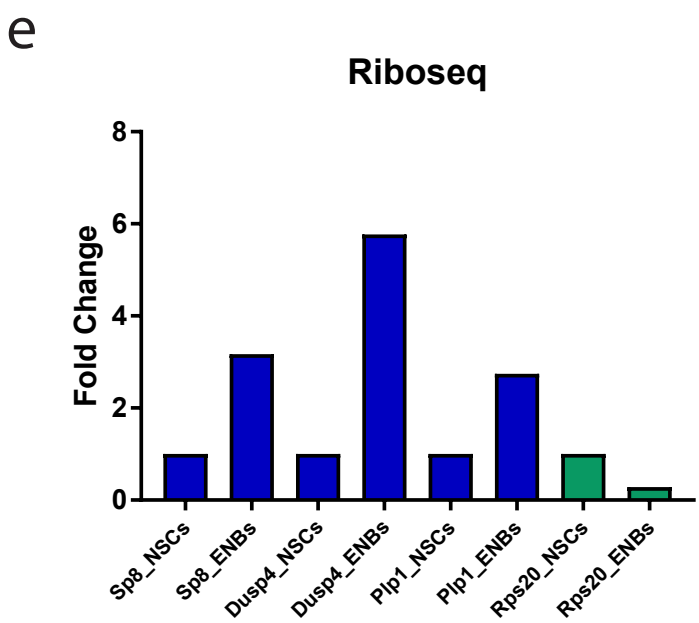

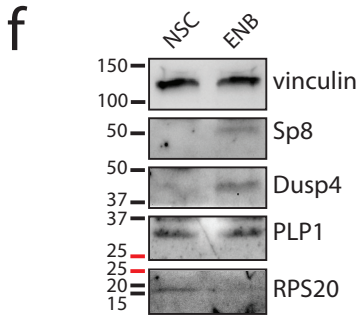

Extended Data Figure 5

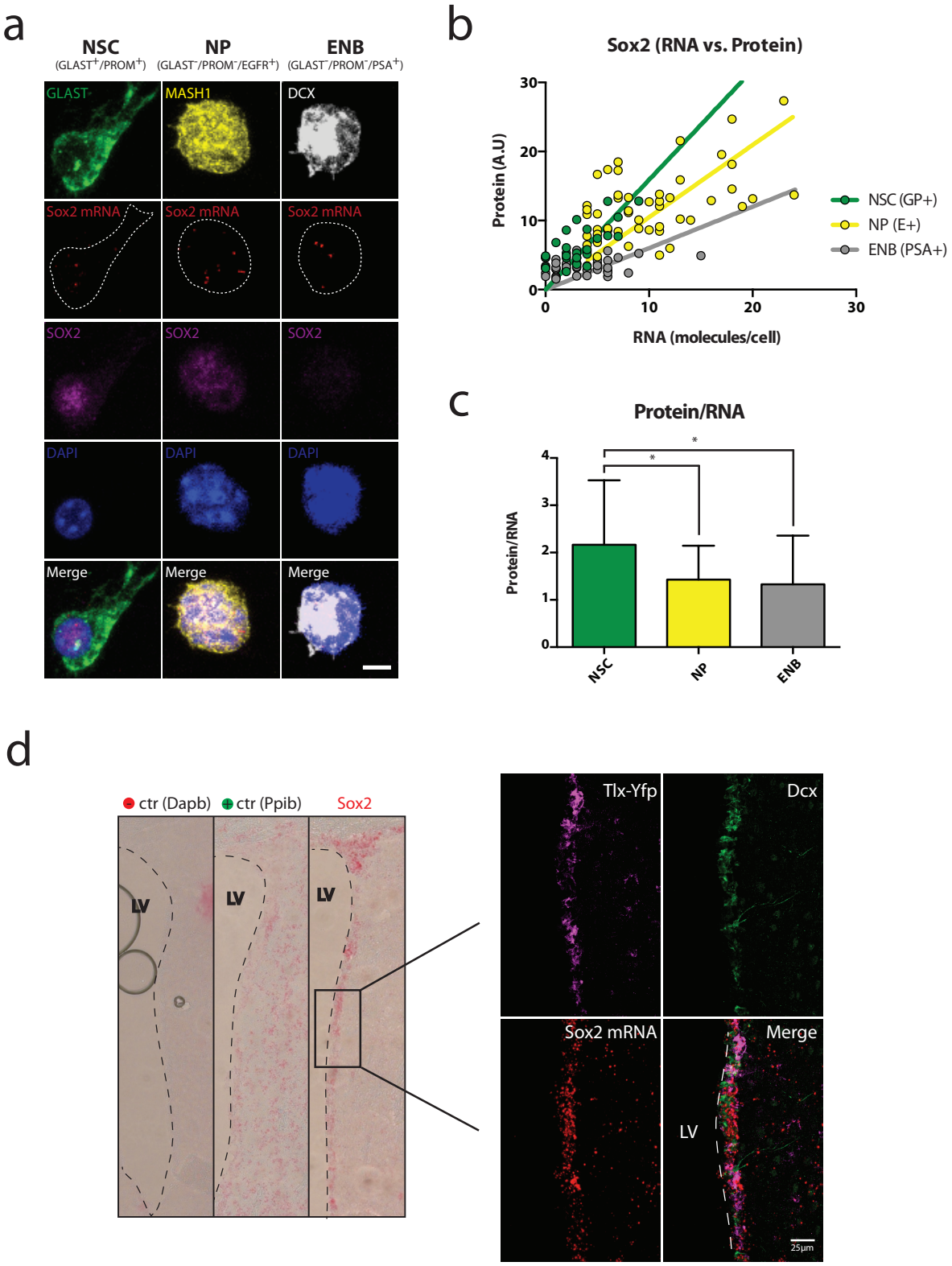

Extended Data Figure 6

a

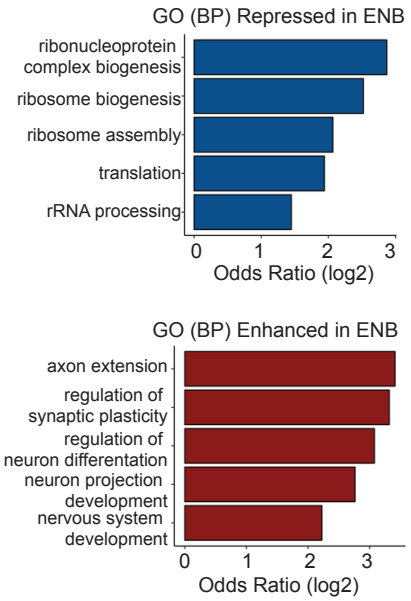

b

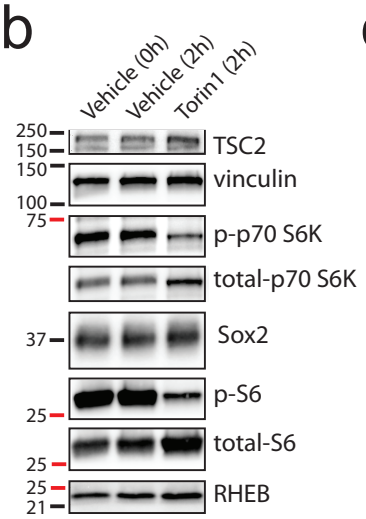

c

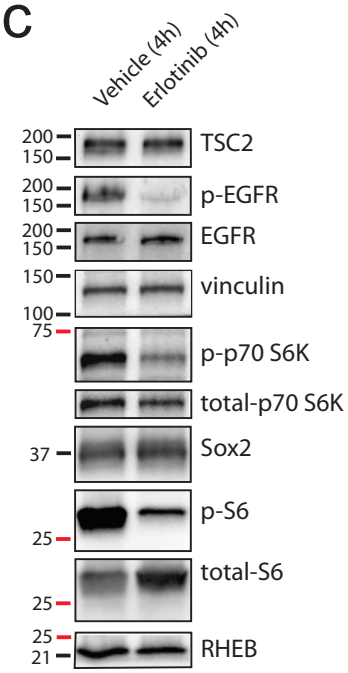

d

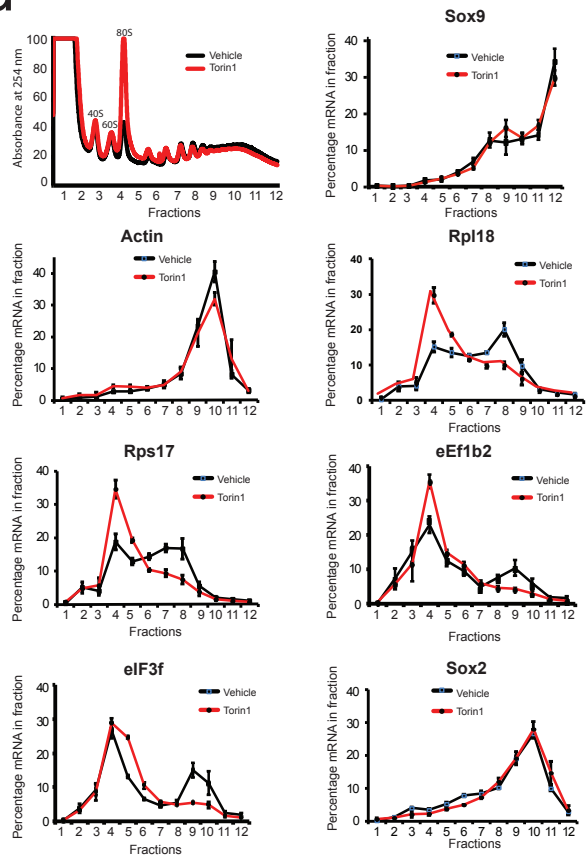

e

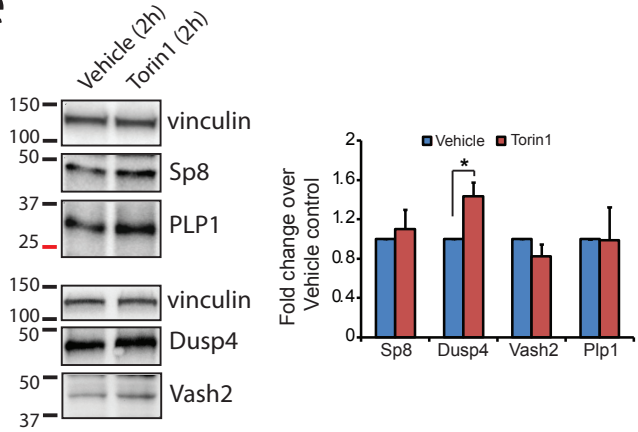

f

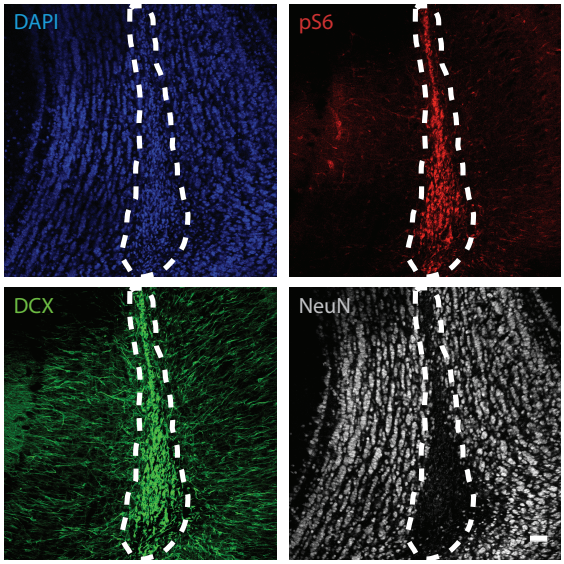
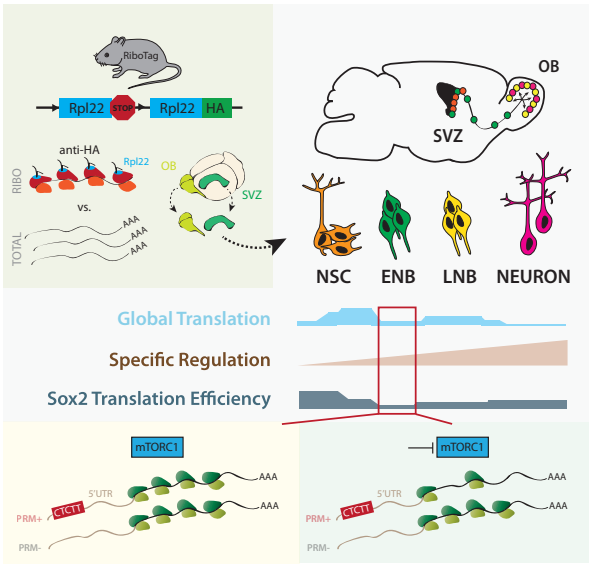
g